A contour algorithm for computing stable fiber bundles of nonautonomous, noninvertible maps

Thorsten Hüls*
Department of Mathematics, Bielefeld University
POB 100131, 33501 Bielefeld, Germany
huels@math.uni-bielefeld.de

March 3, 2016

Abstract

Stable fiber bundles are the nonautonomous analog of stable manifolds and these objects provide valuable information on the underlying dynamics. We propose an algorithm for their computation that applies to a wide class of models, including noninvertible and nonautonomous discrete time systems. Precise error estimates are provided and fiber bundles are computed for several examples.

Keywords: Invariant fiber bundles, discrete time dynamical systems, noninvertible and nonautonomous dynamics, numerical approximation, contour method.
AMS Subject Classification: 37B55, 37D10, 65Q10.

1 Introduction

The stable manifold of a fixed point ξ in a discrete time dynamical system

$$x_{n+1} = F(x_n), \quad n \in \mathbb{Z}, \quad F(\xi) = \xi, \text{ with a diffeomorphism } F : \mathbb{R}^d \to \mathbb{R}^d \quad (1)$$

consists of all points that converge in forward time towards ξ, i.e.

$$W^s(\xi) = \{x \in \mathbb{R}^d : \lim_{n\to\infty} F^n(x) = \xi\}.$$

Due to their dynamical importance, several techniques have been developed to obtain accurate numerical approximations. It is the aim of this paper to introduce an approach that applies – unchanged – to autonomous and nonautonomous

*Supported by CRC 701 'Spectral Structures and Topological Methods in Mathematics' and RCM^2 'Research Centre for Mathematical Modelling'.

systems that are invertible or noninvertible. We are mainly interested in graphically illustrating stable manifolds, and thus, restrict ourselves to space dimension $d \in \{2, 3\}$.

For discrete time systems, the simplest idea to approximate a stable manifold lies in choosing several starting points on the stable subspace of $F'(\xi)$ (shifted by ξ) and iterate them backward in time, using the inverse mapping. More elaborate methods are based of continuation techniques, for example, the search circle algorithm in [45] and refined versions that also work for noninvertible maps [24, 25]. Alternatively, a set oriented subdivision algorithm like GAIO, cf. [19], applies for computing invariant objects and particularly stable and unstable manifolds [20]. We refer to [46] for an overview on numerical methods for computing two-dimensional manifolds in continuous time.

Denote by $X^{s,u}$ the stable and unstable subspaces of $F'(\xi)$, respectively. It is well known that the stable manifold can locally be expressed as the graph of a function $h : X^s \to X^u$:

$$W^s_{\text{loc}} = \{\xi + x_s + h(x_s) : x_s \in X^s \cap U\}, \tag{2}$$

where U is a sufficiently small neighborhood of the origin, see [26, 34, 41, 52, 53, 62, 65]. Differentiating the corresponding invariance condition leads to Taylor expansions of the local graph representation that have been numerically computed by several authors, cf. e.g. [11, 23, 47]. A related approach for establishing existence and regularity of invariant manifold is the so called parameterization method, see [13]. Solving an invariance condition by calculating its coefficients numerically, results in approximate manifolds, cf. [18].

In nonautonomous systems, local Taylor approximations of invariant fibers have been computed for discrete time models in [58] and for continuous time systems, we refer to [59]. These references particularly focus on detecting coefficients of nonautonomous bifurcations. Finally, we note that the calculation of fixed points of the Lyapunov-Perron operator results in alternative approximations of invariant fibers, see [60] and [61].

The idea that we pursue here is based on Hadamard's graph transform, cf. [28], [44, Hadamard-Perron Theorem 6.2.8]. In this introduction, we present our ansatz for invertible, autonomous systems (1). Assume that $\xi = 0$ is a fixed point of F and that the graph representation (2) of the stable manifold is global. Further assume that X^s and X^u are adjusted to the coordinate axes (apply cut off techniques and a transformation, otherwise). Choose $g_0(x_s) = 0$ for all $x_s \in X^s$ and iterate

$$\text{graph}(g_m) = F^{-1}(\text{graph}(g_{m-1})), \quad m = 1, 2, \ldots. \tag{3}$$

Then, it is well known from the contraction mapping principle that g_m converges towards h as $m \to \infty$, see Figure 1.

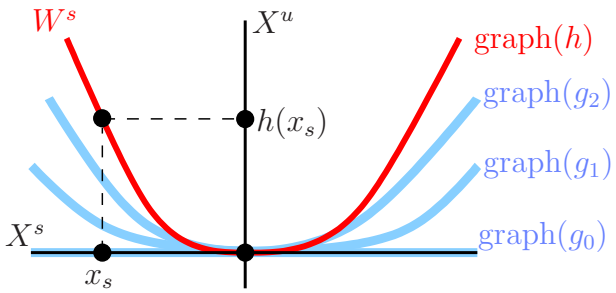

Figure 1: Hadamard's graph transform.

Equation (3) can be rewritten as

$$F^m(\text{graph}(g_m)) = \text{graph}(g_0) \quad \text{and thus} \quad F^m \begin{pmatrix} x_s \\ g_m(x_s) \end{pmatrix} = \begin{pmatrix} * \\ 0 \end{pmatrix} \text{ for all } x_s \in X^s.$$

The next step is the computation of the zero-contour

$$C_m := \left\{ x \in \mathbb{R}^d : \left(F^m \begin{pmatrix} x_s \\ x_u \end{pmatrix} \right)_u = 0 \right\}, \tag{4}$$

where the index u denotes a restriction to the unstable subspace. For sufficiently large m, it turns out that C_m is an accurate approximation of the graph of the unknown function h. Consequently, we obtain in this way a precise picture of the stable manifold W^s.

The structure of this paper is as follows. In Section 2, we discuss appropriate notions of hyperbolicity for nonautonomous systems. Exponential dichotomies provide this stability information and we introduce them in an infinite- and a finite-time setup. In addition, techniques are cited for computing finite-time invariant fibers, which are generally "fat" objects. Note that the theoretical background differs substantially in finite and infinite-time, while numerical methods apply to both cases.

The main objective of this paper is the finite approximation of stable fibers, defined through infinite-time dynamical systems. A new method is constructed in Section 3, by generalizing the idea from above, to a nonautonomous setup. We justify this approach for noninvertible, nonautonomous difference equations by proving upper semicontinuity of C_m and additionally stating precise estimates on the errors involved. An efficient implementation of the contour algorithm is discussed in Section 4. To make it applicable to a wide class of models, we implement it for nonautonomous systems. Furthermore, we replace fixed points by bounded trajectories and allow tangent spaces of fiber bundles to lie arbitrarily in space.

In Section 5 we introduce several autonomous and nonautonomous, invertible and noninvertible models. These models show various difficulties like rich and

even chaotic dynamics, two-dimensional stable manifolds, self-intersections of stable fibers and stable fibers, which have the form of one or more closed loops.

For all systems treated here, our algorithm successfully applies. Finally, error estimates are verified numerically for a test example, having stable fibers with an explicitly given global graph representation.

2 Notions of hyperbolicity

Before we continue in Section 3 with the development of our method for computing stable fibers, we discuss basic notions of stability in this section.

It is well known that for autonomous linear difference equations

$$u_{n+1} = Au_n, \quad A \in \mathbb{R}^{d,d}, \quad n \in \mathbb{Z},$$

the spectrum $\sigma(A)$ provides complete information on the underlying dynamics. All points from the generalized eigenspace w.r.t. the stable eigenvalues $\lambda \in \sigma(A)$, $|\lambda| < 1$ converge towards the fixed point 0. On the other hand, points from the unstable eigenspace X^u converge backward in time towards 0.

This situation changes dramatically when considering linear nonautonomous systems of the form

$$u_{n+1} = A_n u_n, \quad A_n \in \mathbb{R}^{d,d}, \quad n \in \mathbb{Z}. \tag{5}$$

In this context, eigenvalues are generally useless for analyzing stability properties of the fixed point 0. A famous counter example is due to Vinograd, cf. [15, Section 2.6].

Starting with the groundbreaking work of Perron [56], the theory of exponential dichotomies provides the desired stability information. We refer to the monographs [16, 17] and [33, Definition 7.6.1] and follow the latter reference for introducing dichotomies in a noninvertible setup. Denote by Φ the solution operator of (5), defined as

$$\Phi(n,m) = \begin{cases} A_{n-1} \cdot \ldots \cdot A_m, & \text{for } n > m, \\ I, & \text{for } n = m. \end{cases}$$

Definition 1 *The difference equation* (5) *has an* ***exponential dichotomy*** *with data* $(K, \alpha_{s,u}, P_n^{s,u})$ *on* $\mathbb{Z}$*, if constants* $K, \alpha_s, \alpha_u > 0$ *and families of projectors* P_n^s*,* $P_n^u := I - P_n^s$*,* $n \in \mathbb{Z}$ *exist such that*

(i) $P_n^{s,u}\Phi(n,m) = \Phi(n,m)P_m^{s,u}$ *for all* $n, m \in \mathbb{Z}$*,* $n \geq m$*,*

(ii) $A_n|_{\mathcal{R}(P_n^u)} : \mathcal{R}(P_n^u) \to \mathcal{R}(P_{n+1}^u)$ *is invertible for all* $n \in \mathbb{Z}$ *and denote by* $\bar{\Phi}(m,n) : \mathcal{R}(P_n^u) \to \mathcal{R}(P_m^u)$*,* $n \geq m$ *the inverse of* $\Phi(n,m)|_{\mathcal{R}(P_m^u)}$*.*

(iii) For $n, m \in \mathbb{Z}$, $n \geq m$ the following estimates hold true:

$$\|\Phi(n,m)P^s_m\| \leq K\mathrm{e}^{-\alpha_s(n-m)}, \quad \|\bar{\Phi}(m,n)P^u_n\| \leq K\mathrm{e}^{-\alpha_u(n-m)}.$$

Note that condition (ii) guarantees regularity of the difference equation in the unstable direction. A dichotomy of this type is called regular in [4, Definition 3.1] and [42].

Exponential dichotomies capture asymptotic dynamics of nonautonomous systems. Transient effects are hidden in the constant K. These transient dynamics turn out to be particularly significant for applications, given on a finite-time horizon. Important examples are Lagrangian coherent structures in fluid flow models, cf. [31] and the references therein.

Corresponding stability notions are finite-time exponential dichotomies that have been developed in [8], [7, Definition 2], [21, Definition 1]. A meaningful definition of hyperbolicity in finite-time requires $K = 1$ for the dichotomy constant in Definition 1 and condition (iii) reads

$$\begin{aligned} \|\Phi(n,m)x\| &\leq \mathrm{e}^{-\alpha_s(n-m)}\|x\| \quad \text{for all } x \in \mathcal{R}(P^s_m),\ n \geq m, \\ \|\Phi(n,m)x\| &\geq \mathrm{e}^{\alpha_u(n-m)}\|x\| \quad \text{for all } x \in \mathcal{R}(P^u_m),\ n \geq m. \end{aligned} \tag{6}$$

For this notion of hyperbolicity, a spectral theory has been developed in [7] in continuous time.

A method for computing finite-time invariant manifolds in two dimensional velocity fields $x' = f(x,t)$ is suggested in [29]. Denote by $x(\cdot, x_0)$ the solution with initial value x_0 at time t_0. The approach is based on computing local maxima w.r.t. x_0 of $\{t : \det D_x f(x(\tau, x_0), \tau) < 0 \text{ for all } t_0 \leq \tau < t\}$.

Alternatively, the authors of [49] grow stable and unstable fiber bundles from a local approximation via backward and forward iterations, respectively. For the development of the theoretical background of nonautonomous fiber bundles in finite-time, we refer to [22].

On an infinite-time horizon, dichotomies do not depend on the chosen norm. This contrasts the finite-time setup, where a carefully selected norm is essential. Furthermore, transient effects in the center of a finite interval cannot be compensated, since (6) guarantees strict monotony w.r.t. the chosen norm. Due to this monotony, this dichotomy concept is called M-hyperbolicity. In addition, further nonequivalent finite-time notions have been introduced, see [30] and [6].

Finite-time conditions that guarantee an exponential dichotomy on $\mathbb{Z}$ in the sense of Definition 1 are given in [55, Theorem 2.1]. These conditions are exponential dichotomies with a sufficiently small constant $K \geq 1$ on all sufficiently large finite intervals $[b, b+\ell]$ with b from a relatively dense set of $\mathbb{Z}$. Slowly varying systems and almost periodic systems are two classes of models, satisfying these assumptions.

In this paper we consider the infinite-time setup from Definition 1. Approximations of stable fibers are computed numerically on finite intervals and occurring errors are analyzed in detail.

3 Approximation of stable fiber bundles

In this section nonautonomous systems that may be noninvertible are considered and basic assumptions are stated. We generalize the contour method (4) to this nonautonomous setup and present a rigorous justification, including error estimates.

3.1 Setup

Consider a nonautonomous discrete time dynamical system in $\mathbb{R}^d$ of the form

$$x_{n+1} = F_n(x_n), \quad n \in \mathbb{Z}, \tag{7}$$

where $F_n \in \mathcal{C}^2(\mathbb{R}^d, \mathbb{R}^d)$ and

$$\Psi(n,m) := \begin{cases} F_{n-1} \circ \ldots \circ F_m, & \text{for } n > m, \\ I, & \text{for } n = m \end{cases}$$

defines the solution operator of (7), transferring the solution from time m to time n for $n \geq m$. We assume that the maps F_n have a common fixed point 0 and a block structure, i.e. with $d = d_s + d_u$ it holds for all $n \in \mathbb{Z}$ that

$$F_n(0) = 0, \quad DF_n(0) = \begin{pmatrix} A_n^s & 0 \\ 0 & A_n^u \end{pmatrix} \text{ with matrices } A_n^s \in \mathbb{R}^{d_s,d_s},\ A_n^u \in \mathbb{R}^{d_u,d_u}.$$

On the one hand, these are rather strong assumptions. On the other hand, a similarity transform leads to the proposed structure under reasonable assumptions. The general case is analyzed in detail in Section 4.

Decompose $x = \begin{pmatrix} x_s \\ x_u \end{pmatrix}$, $x_s \in \mathbb{R}^{d_s}$, $x_u \in \mathbb{R}^{d_u}$. We assume that

(A1) $F_n(x) = \begin{pmatrix} A_n^s x_s + f_n^s(x_s, x_u) \\ A_n^u x_u + f_n^u(x_s, x_u) \end{pmatrix}$ for $n \in \mathbb{Z}$, where the matrices $A_n^u \in \mathbb{R}^{d_u,d_u}$ are invertible with uniformly bounded inverse,
$A_n^s \in \mathbb{R}^{d_s,d_s}$, $f_n^{s,u} \in \mathcal{C}^1(\mathbb{R}^d, \mathbb{R}^{d_{s,u}})$, $f_n^{s,u}(0) = 0$ and $Df_n^{s,u}(0) = 0$.

Denote by Φ^u the solution operator of the linear difference equation $u_{n+1} = A_n^u u_n$, $n \in \mathbb{Z}$ and let $\Phi^s(n,m)$, $n \geq m$ be the solution operator of $u_{n+1} = A_n^s u_n$, which is only defined in forward time. The following assumption establishes an exponential dichotomy of the variational equation

$$u_{n+1} = DF_n(0)u_n, \quad n \in \mathbb{Z}, \tag{8}$$

see Definition 1.

(A2) There exist constants $K, \alpha_s, \alpha_u > 0$, such that the estimates

$$\|\Phi^s(n,m)\| \leq K\mathrm{e}^{-\alpha_s(n-m)}, \quad \|\Phi^u(m,n)\| \leq K\mathrm{e}^{-\alpha_u(n-m)}.$$

hold true for all $n \geq m$, $n, m \in \mathbb{Z}$.

Further assume that the following assertions hold uniformly for $n \in \mathbb{Z}$.

(A3) For all $\varepsilon > 0$ there exists a neighborhood U of 0 such that $\|Df_n^{s,u}(x)\| \leq \varepsilon$ for all $x \in U$ and for all $n \in \mathbb{Z}$.

(A4) On each compact set $\mathcal{K} \subset \mathbb{R}^d$, there exists a constant $L_{\mathcal{K}} > 0$ such that F_n^{-1} is uniformly Lipschitz in a set-valued sense, i.e.

$$F_n^{-1}(x) \subset F_n^{-1}(y) + L_{\mathcal{K}}\|x-y\|B \text{ for all } x, y \in \mathcal{K},\ n \in \mathbb{Z},$$

where B denotes the unit ball in $\mathbb{R}^d$, see [1, Definition 1.4.5].

3.2 Stable fiber bundles

Assuming **(A1)**–**(A3)**, we define the notion of global stable fibers of (7) w.r.t. the fixed point 0 at time k as

$$\mathcal{F}_k := \{x \in \mathbb{R}^d : \lim_{m\to\infty} \Psi(m,k)x = 0\}.$$

Note that stable fibers are invariant in forward time in the following sense

$$x \in \mathcal{F}_k \Rightarrow \Psi(m,k)x \in \mathcal{F}_m \quad \text{for all } m \geq k. \tag{9}$$

In a sufficiently small neighborhood U of 0, the local fiber

$$\mathcal{F}_k^{\mathrm{loc}} := \{x \in \mathbb{R}^d : \Psi(m,k)x \in U \text{ for } m \geq k, \lim_{m\to\infty} \Psi(m,k)x = 0\}$$

can be expressed as the graph of a function $h_k \in \mathcal{C}^1(\mathbb{R}^{d_s}, \mathbb{R}^{d_u})$:

$$\mathcal{F}_k^{\mathrm{loc}} = \{(x_s, h_k(x_s))^T, x_s \in \mathbb{R}^{d_s} \cap U_s\}. \tag{10}$$

Additionally, $h_k(0) = 0$, h_k is Lipschitz, uniformly w.r.t. k, i.e. in a sufficiently small neighborhood $U_s \subset \mathbb{R}^{d_s}$ of 0, we get

$$\|h_k(x_s)\| \leq L_h\|x_s\| \quad \text{for all} \quad x_s \in U_s, \quad k \in \mathbb{Z}. \tag{11}$$

Furthermore, $Dh_k(0) = 0$, see [2, Theorem 4.1], [5, Theorem 4.11], [57, Theorem 4.6.4].

An alternative characterization of global stable fibers that are the continuations of the local ones, is given in

Theorem 2 *Assume* **(A1)**–**(A3)**. *Then there exists a $\delta > 0$ such that for any $k \in \mathbb{Z}$*

$$\mathcal{F}_k = \mathcal{S}_k^\delta := \{x \in \mathbb{R}^d : \exists M > k : \Psi(m,k)x \in B_\delta \ \forall m \geq M\}, \tag{12}$$

where $B_\delta = \{x \in \mathbb{R}^d : \|x\| \leq \delta\}$.

This assertion is well known in the autonomous case, see [62, Theorem III.7] and for nonautonomous systems, we refer to [57, Corollary 4.6.11]. For the reader's convenience, we present a direct proof. We start by analyzing one iteration of (7) in a neighborhood of the fixed point 0.

Lemma 3 *Assume* **(A1)**–**(A3)**. *For any $\varepsilon > 0$ there exists a $\delta > 0$, such that the following assertion holds true.*

Fix $m \in \mathbb{Z}$ and let

$$x = \begin{pmatrix} x_s \\ h_m(x_s) + \ell_m \end{pmatrix} \in B_\delta, \quad x_s \in \mathbb{R}^{d_s}, \ \ell_m \in \mathbb{R}^{d_u},$$

such that

$$\begin{pmatrix} x_s \\ h_m(x_s) \end{pmatrix} \in B_\delta \quad \textit{and} \quad y := F_m(x) \in B_\delta.$$

Decompose

$$y = \begin{pmatrix} y_s \\ h_{m+1}(y_s) + \ell_{m+1} \end{pmatrix}, \quad y_s \in \mathbb{R}^{d_s}, \ \ell_{m+1} \in \mathbb{R}^{d_u} \tag{13}$$

and assume that

$$\begin{pmatrix} y_s \\ h_{m+1}(y_s) \end{pmatrix} \in B_\delta. \tag{14}$$

Then $\ell_{m+1} = \tilde{A}_m^u \ell_m$ with some matrix $\tilde{A}_m^u \in \mathbb{R}^{d_u, d_u}$, satisfying $\|\tilde{A}_m^u - A_m^u\| \leq \varepsilon$.

Proof: Let $\varepsilon > 0$. Utilizing Assumption **(A3)**, we find a $\delta > 0$ such that

$$\begin{aligned} \|D_2 f_n^{s,u}(x_s, x_u)\| &\leq \tfrac{\varepsilon}{2} \text{ for all } \begin{pmatrix} x_s \\ x_u \end{pmatrix} \in B_\delta, \\ \|Dh_n(x_s)\| &\leq 1 \text{ for all } \|x_s\| \leq \delta + \delta\varepsilon \end{aligned} \tag{15}$$

holds true for all $n \in \mathbb{Z}$. By choosing $m \in \mathbb{Z}$ and assuming **(A1)**, we obtain

$$\begin{aligned} F_m \begin{pmatrix} x_s \\ h_m(x_s) + \ell_m \end{pmatrix} &= \begin{pmatrix} A_m^s x_s + f_m^s(x_s, h_m(x_s) + \ell_m) \\ A_m^u h_m(x_s) + A_m^u \ell_m + f_m^u(x_s, h_m(x_s) + \ell_m) \end{pmatrix} \\ &= \begin{pmatrix} A_m^s x_s + f_m^s(x_s, h_m(x_s)) + B_1^m(\ell_m)\ell_m \\ A_m^u h_m(x_s) + f_m^u(x_s, h_m(x_s)) + A_m^u \ell_m + B_2^m(\ell_m)\ell_m \end{pmatrix}, \end{aligned}$$

where

$$B_1^m(\ell) := \int_0^1 D_2 f_m^s(x_s, h_m(x_s) + \tau\ell) d\tau, \quad B_2^m(\ell) := \int_0^1 D_2 f_m^u(x_s, h_m(x_s) + \tau\ell) d\tau.$$

By defining $\tilde{y}_s = A^s_m x_s + f^s_m(x_s, h_m(x_s))$ and using the invariance of stable fibers (9) we get

$$\begin{aligned} F_m(x) &= \begin{pmatrix} \tilde{y}_s + B^m_1(\ell_m)\ell_m \\ h_{m+1}(\tilde{y}_s) + B^m_2(\ell_m)\ell_m + A^u_m \ell_m \end{pmatrix} \\ &= \begin{pmatrix} \tilde{y}_s + B^m_1(\ell_m)\ell_m \\ h_{m+1}(\tilde{y}_s + B^m_1(\ell_m)\ell_m) + B^m_2(\ell_m)\ell_m + A^u_m \ell_m + B^m_3(\ell_m)\ell_m \end{pmatrix} \\ &= \begin{pmatrix} y_s \\ h_{m+1}(y_s) + \tilde{A}^u_m \ell_m \end{pmatrix} = \begin{pmatrix} y_s \\ h_{m+1}(y_s) + \ell_{m+1} \end{pmatrix}, \end{aligned}$$

with

$$\begin{aligned} B^m_3(\ell_m) &= -\int_0^1 Dh_{m+1}(\tilde{y}_s + \tau B^m_1(\ell_m)\ell_m) d\tau B^m_1(\ell_m), \\ y_s &= \tilde{y}_s + B^m_1(\ell_m)\ell_m, \\ \tilde{A}^u_m &= A^u_m + B^m_2(\ell_m) + B^m_3(\ell_m), \\ \ell_{m+1} &= \tilde{A}^u_m \ell_m. \end{aligned}$$

Note that (13), (14) and (15) yield

$$\sup_{\tau\in[0,1]} \|\tilde{y}_s + \tau B^m_1(\ell_m)\ell_m\| \le \|y_s\| + \sup_{\tau\in[0,1]} (1-\tau)\|B^m_1(\ell_m)\|\|\ell_m\| \le \delta + \frac{\varepsilon}{2}\cdot 2\delta = \delta + \delta\varepsilon.$$

Hence we conclude that

$$\|\tilde{A}^u_m - A^u_m\| \le \|B^m_2(\ell_m)\| + \|B^m_3(\ell_m)\| \le \tfrac{\varepsilon}{2} + \tfrac{\varepsilon}{2} = \varepsilon.$$

■

Proof of Theorem 2: For $x \in \mathcal{F}_k$ it immediately follows that $x \in \mathcal{S}^\delta_k$ and thus, $\mathcal{F}_k \subset \mathcal{S}^\delta_k$ for all $\delta > 0$.

The proof of $\mathcal{F}_k \supset \mathcal{S}^\delta_k$ first requires a bound on δ.

For $\varepsilon > 0$ sufficiently small, the Roughness-Theorem for exponential dichotomies, cf. [54, Proposition 2.10] applies to the perturbed difference equation

$$u_{n+1} = (A^u_n + E_n)u_n, \quad \|E_n\| \le \varepsilon, \quad n \in \mathbb{Z}. \tag{16}$$

Consequently, there exists for each $0 < \tilde{\alpha}_u < \alpha_u$ a constant $K > 0$, such that the solution operator $\tilde{\Phi}^u$ of (16) can be estimated as

$$\|\tilde{\Phi}^u(m,n)\| \le K\mathrm{e}^{-\tilde{\alpha}_u(n-m)}, \quad n \ge m. \tag{17}$$

We fix this ε and choose δ as in Lemma 3. Further, let $\delta_1 < \delta$ such that

$$\begin{pmatrix} x \\ h_n(x) \end{pmatrix} \in B_\delta \quad \text{for all } n \in \mathbb{Z} \text{ and all } \begin{pmatrix} x \\ 0 \end{pmatrix} \in B_{\delta_1}.$$

For proving $\mathcal{F}_k \supset \mathcal{S}_k^{\delta_1}$ let $z \in \mathcal{S}_k^{\delta_1}$, then there exists an $M \in \mathbb{N}$ such that $\Psi(m,k)z \in B_{\delta_1}$ for all $m \geq M$. We apply Lemma 3 to

$$x = \begin{pmatrix} z_M \\ h_M(z_M) + \ell_M \end{pmatrix} = \Psi(M,k)z,\ y = \begin{pmatrix} z_{M+1} \\ h_{M+1}(z_{M+1}) + \ell_{M+1} \end{pmatrix} = \Psi(M+1,k)z$$

and observe that Assumption (13) is satisfied. It follows that

$$\ell_{M+1} = (A_M^u + E_M)\ell_M,\ \text{with } \|E_M\| = \|B_2^M(\ell_M) + B_3^M(\ell_M)\| \leq \varepsilon.$$

Inductively, we conclude for $m \in \mathbb{N}$

$$\Psi(M+m,k)z = \begin{pmatrix} z_{M+m} \\ h_{M+m}(z_{M+m}) + \tilde{\Phi}^u(M+m,M)\ell_M \end{pmatrix}. \tag{18}$$

Applying (17), we obtain

$$\|\tilde{\Phi}^u(M+m,M)\ell_M\| \geq \tfrac{1}{K}\mathrm{e}^{\tilde{\alpha}_u m}\|\ell_M\| \tag{19}$$

and thus, the left hand side of (19) is for increasing m unbounded for $\ell_M \neq 0$. On the other hand, $\|h_{M+m}(z_{M+m})\|$ is bounded, see (11). Since $\Psi(M+m,k)z \in B_{\delta_1}$ for all $m \geq 0$, it follows from (18) that $\ell_M = 0$ and $z \in \mathcal{F}_k$. ■

3.3 Justification of finite-time computations

The proof of Theorem 2 indicates that the most critical terms occur in the unstable direction. To avoid this problem, we fix δ as in the proof of Theorem 2 and consider for $k \in \mathbb{Z}$, $m,p \in \mathbb{N}$ the set

$$\mathcal{T}_{F,k}^{m,p} := \left\{ x \in \mathbb{R}^d : \Psi(i+p+k,k)x \in B_\delta\ \forall 0 \leq i \leq m, (\Psi(m+p+k,k)x)_u = 0 \right\}. \tag{20}$$

The symbol F in $\mathcal{T}_{F,k}^{m,p}$ gives reference to the family of maps, defining the dynamical system (7). The index k denotes the time, the approximate fiber is computed at. Points in the set $\mathcal{T}_{F,k}^{m,p}$ lie after p iteration steps in B_δ. Thus p controls the length of the fiber. Finally, the next m steps stay in the neighborhood B_δ and it turns out that approximation errors decrease for increasing m.

In the limit $m \to \infty$ we get $\mathcal{T}_{F,k}^{\infty,p} \subset \mathcal{F}_k$, but numerically, $\mathcal{T}_{F,k}^{m,p}$ can only be computed for finite values of m and p. We establish precise error estimates and justify in this way computations at finite-time.

Theorem 4 *Assume* **(A1)**–**(A4)**. *Then, there exist constants $C, \alpha > 0$, $\beta \in \mathbb{R}$, such that for all $k \in \mathbb{Z}$, $m,p \in \mathbb{N}$*

$$\operatorname{dist}(\mathcal{T}_{F,k}^{m,p}, \mathcal{F}_k) \leq C\mathrm{e}^{\beta p} \cdot \mathrm{e}^{-\alpha m}. \tag{21}$$

Here, $\operatorname{dist}(A,B) = \sup_{a\in A}\inf_{b\in B}\|a-b\|$ denotes the Hausdorff semi-distance.
Proof: Choose ε and δ_1 as in the proof of Theorem 2 and fix $m,p\in\mathbb{N}$. For $x\in\mathcal{T}_{F,k}^{m,p}$ let $x_i := \Psi(i+k,k)x$ for $i=0,\dots,p+m$. Then it follows that $x_i\in B_{\delta_1}$ for all $i=p,\dots,m+p$. Rewrite

$$x_{p+i} = \begin{pmatrix} x_{p+i}^s \\ h_{p+i}(x_{p+i}^s)+\ell_{p+i}\end{pmatrix}, \quad i=0,\dots,m$$

and observe that the second condition in the definition of $\mathcal{T}_{F,k}^{m,p}$ leads to

$$x_{p+m} = \begin{pmatrix} x_{p+m}^s \\ 0\end{pmatrix} = \begin{pmatrix} x_{p+m}^s \\ h_{p+m}(x_{p+m}^s)+\ell_{p+m}\end{pmatrix} \text{ with } \ell_{p+m} = -h_{p+m}(x_{p+m}^s). \tag{22}$$

By Lemma 3, we get

$$\ell_{p+i+1} = \tilde{A}_{p+i}^u \ell_{p+i}, \quad i=0,\dots,m-1$$

and inductively it follows

$$\ell_{p+i} = \tilde{\Phi}^u(p+i,p)\ell_p \quad\Leftrightarrow\quad \ell_p = \tilde{\Phi}^u(p,p+i)\ell_{p+i}, \quad i=0,\dots,m.$$

Letting $i=m$ and using (11), (17) and (22), we obtain the estimate

$$\|\ell_p\| \le \|\tilde{\Phi}^u(p,p+m)\|\|\ell_{p+m}\| \le K\mathrm{e}^{-\tilde{\alpha}_u m}\|h_{p+m}(x_{p+m}^s)\| \le KL_h\mathrm{e}^{-\tilde{\alpha}_u m}\|x_{p+m}^s\|. \tag{23}$$

In a sufficiently small δ-neighborhood, it follows from the Roughness-Theorem for regular exponential dichotomies (cf. [3, Theorem 4.4]) that

$$\|x_{p+m}^s\| \le \tilde{C}\mathrm{e}^{-\tilde{\alpha}_s m}, \quad \text{with some} \quad \tilde{C}>0, \quad 0<\tilde{\alpha}_s<\alpha_s.$$

Combining this result with (23) yields $\|\ell_p\| \le \tilde{C}KL_h\mathrm{e}^{-(\tilde{\alpha}_s+\tilde{\alpha}_u)m}$.

We choose a sufficient large compact set $\mathcal{K}$. From **(A4)** we conclude existence of a pre-image $y\in\mathcal{F}_k$ with $\Psi(p+k,k)y = \begin{pmatrix} x_p^s \\ h_p(x_p^s)\end{pmatrix}$ and

$$x_i = \Psi(i+k,k)x \in \mathcal{K}, \quad y_i := \Psi(i+k,k)y \in \mathcal{K} \quad \text{for all } i=0,\dots,p,$$

satisfying

$$\|x_i-y_i\| \le L_{\mathcal{K}}^{p-i}\|x_p-y_p\| = \mathrm{e}^{(p-i)\ln L_{\mathcal{K}}}\|\ell_p\| \quad i=0,\dots,p.$$

Here, $L_{\mathcal{K}}$ is the Lipschitz constant, introduced in **(A4)**. Consequently, we get the estimate (21) with the setting $C=\tilde{C}KL_h$, $\beta=\ln L_{\mathcal{K}}$, $\alpha=\tilde{\alpha}_s+\tilde{\alpha}_u$, i.e.

$$\operatorname{dist}(x,\mathcal{F}_k) \le \|x_0-y_0\| \le C\mathrm{e}^{\beta p}\cdot\mathrm{e}^{-\alpha m}$$

holds true for all $x\in\mathcal{T}_{F,k}^{m,p}$ and the proof is complete. ■

For fixed k and p, Theorem 4 shows that $\operatorname{dist}(\mathcal{T}_{F,k}^{m,p},\mathcal{F}_k)\to 0$ as $m\to\infty$, i.e. $\mathcal{T}_{F,k}^{m,p}$ is upper-semicontinuous, with an exponential rate of convergence. For the examples in Section 5.3 and Section 5.7 we get improved versions of (21) by exploiting their special structure. Consecutive numerical tests indicate that these rates of convergence are sharp.

4 Implementation of the contour algorithm

In this section, we introduce an algorithm for computing the set $T_{F,k}^{m,p}$ numerically. First, we relax Assumption **(A1)**, so that generic cases can be tackled easily.

4.1 The general case

One can hardly expect to find an n-independent fixed point in the nonautonomous dynamical system

$$y_{n+1} = G_n(y_n), \quad G_n \in \mathcal{C}^2(\mathbb{R}^d, \mathbb{R}^d), \quad n \in \mathbb{Z}. \tag{24}$$

The only meaningful replacement is a bounded trajectory, cf. [48]. Furthermore, stable and unstable subspaces are typically not aligned to the coordinate axes. We treat this case by considering the associated equation of perturbed motion. This transformation results in an n-independent fixed point and aligned subspaces. We assume:

(A5) Let $\bar{y}_{\mathbb{Z}}$ be a bounded solution of (24) such that the variational equation

$$u_{n+1} = DG_n(\bar{y}_n)u_n, \quad n \in \mathbb{Z} \tag{25}$$

has an exponential dichotomy with data $(K, \alpha_{s,u}, P_n^{s,u})$ on $\mathbb{Z}$.

Assuming **(A5)**, we transform the system into the setup from Section 3. Consider for $n \in \mathbb{Z}$ the matrices $S_n := \begin{pmatrix} \mathcal{B}(P_n^s) & \mathcal{B}(P_n^u) \end{pmatrix}$, where $\mathcal{B}(P_n^{s,u})$ are bases of $\mathcal{R}(P_n^{s,u})$. We define

$$x_n := S_n^{-1}(y_n - \bar{y}_n), \quad n \in \mathbb{Z} \tag{26}$$

and obtain the transformed system

$$x_{n+1} = F_n(x_n) := S_{n+1}^{-1}\big(G_n(S_n x_n + \bar{y}_n) - \bar{y}_{n+1}\big), \quad n \in \mathbb{Z}. \tag{27}$$

Let Ξ and Ψ be the solution operators of (24) and (27), respectively. Inductively we find

$$\Psi(n,m)x = S_n^{-1}\big(\Xi(n,m)(S_m x + \bar{y}_m) - \bar{y}_n\big), \quad n \geq m. \tag{28}$$

As a consequence, 0 is a time independent fixed point of (27) and the corresponding variational equation reads

$$u_{n+1} = DF_n(0)u_n = S_{n+1}^{-1} DG_n(\bar{y}_n) S_n u_n, \quad n \in \mathbb{Z}. \tag{29}$$

Note that the two systems (25) and (29) turn into each other via a nonautonomous similarity transformation. The exponential dichotomy of (25) that

we assume in **(A5)** carries over to equation (29). Corresponding data are given as $(K, \alpha_{s,u}, Q^{s,u})$, with n-independent projectors

$$Q^s := S_n^{-1} P_n^s S_n = \begin{pmatrix} I_s & 0 \\ 0 & 0 \end{pmatrix}, \quad Q^u := S_n^{-1} P_n^u S_n = \begin{pmatrix} 0 & 0 \\ 0 & I_u \end{pmatrix}, \quad n \in \mathbb{Z}$$

and identities $I_{s,u}$ of dimension $\dim(\mathcal{R}(P_n^{s,u}))$, respectively. Using Taylor's expansion, $F_n(x) = DF_n(0)x + r_n(x)$, $r_n(x) = \mathcal{O}(\|x\|^2)$, where the constant in the $\mathcal{O}$-estimate may depend on n. We observe that Assumptions **(A1)** and **(A2)** are satisfied. Uniformity w.r.t. n does not follow from **(A5)**. Therefore, we additionally assume **(A3)** with the setting $f_n^{s,u} := r_n|_{\mathcal{R}(Q^{s,u})}$ as well as **(A4)**.

4.2 Fiber bundles in the general case

Let the assumptions from Section 4.1 be fulfilled. Fiber bundles w.r.t. the bounded trajectory $\bar{y}_{\mathbb{Z}}$ are defined as

$$\mathcal{F}_k(\bar{y}_{\mathbb{Z}}) := \{y \in \mathbb{R}^d : \lim_{m\to\infty} \|\Xi(k+m,k)y - y_{k+m}\| = 0\}.$$

In order to compute this set, we first revisit the transformation from Section 4.1 and approximate $\mathcal{T}_{F,k}^{m,p}$ for the transformed system (27). For our numerical experiments in Section 5, we choose δ rather large, set $p = 0$ and only solve the second condition in (20) by computing

$$\tilde{\mathcal{T}}_{F,k}^{m} := \{x \in \mathcal{K} : \tilde{Q}^u \Psi(k+m,k)x = 0\}, \quad \text{with} \quad \tilde{Q}^u = \begin{pmatrix} 0 & I_u \end{pmatrix},$$

in some compact set $\mathcal{K}$. Using (28), we get a representation of $\tilde{\mathcal{T}}_{F,k}^{m}$ in terms of the original system (25):

$$\tilde{\mathcal{T}}_{F,k}^{m} = \{x \in \mathcal{K} : \tilde{Q}^u S_{k+m}^{-1}\big(\Xi(k+m,k)(S_k x + \bar{y}_k) - \bar{y}_{k+m}\big) = 0\}.$$

Applying the inverse transformation (26) we finally obtain an approximation of $\mathcal{F}_k(\bar{y}_{\mathbb{Z}})$:

$$\begin{aligned} \tilde{\mathcal{T}}_{G,k}^{m} &:= \{S_k x + \bar{y}_k,\ x \in \mathcal{K} : \tilde{Q}^u S_{k+m}^{-1}\big(\Xi(k+m,k)(S_k x + \bar{y}_k) - \bar{y}_{k+m}\big) = 0\} \\ &= \{y \in \tilde{\mathcal{K}} : \tilde{Q}^u S_{k+m}^{-1}\big(\Xi(k+m,k)y - \bar{y}_{k+m}\big) = 0\}, \end{aligned} \tag{30}$$

with $\tilde{\mathcal{K}} = \{S_k x + \bar{y}_k : x \in \mathcal{K}\}$.

4.3 The algorithm

After these preparations, we have all tools at hand to state our algorithm for the computation of $\tilde{\mathcal{T}}_{G,k}^{m}$, which is an approximation of the stable fiber $\mathcal{F}_k(\bar{y}_{\mathbb{Z}})$ of (24). For two-dimensional systems, we additionally provide MATLAB code snippets of the single steps of the algorithm. These steps are:

(1) *Approximation of the bounded trajectory* $\bar{y}_{\mathbb{Z}}$.

With **(A5)** we deduce that the bounded solution $\bar{y}_{\mathbb{Z}}$ of (24) is isolated in the Banach space $\mathcal{S} = \{(x_n)_{n\in\mathbb{Z}} \in (\mathbb{R}^d)^{\mathbb{Z}} : \sup_{n\in\mathbb{Z}} \|x_n\| < \infty\}$.

For an approximation of this solution, we setup the boundary value problem on a finite interval $J = [\ell_-, \ell_+] \cap \mathbb{Z}$:

$$\begin{aligned} y_{k+n+1} &= G_{k+n}(y_{k+n}), \quad n = \ell_-, \dots, \ell_+ - 1, \\ y_{k+\ell_-} &= y_{k+\ell_+}. \end{aligned} \tag{31}$$

Numerically, a solution of this nonlinear system is calculated using Newton's method. We refer to [38, Section 2.1] for a justification of this ansatz. Note that we search for an approximation of $\bar{y}_n$ for indices n, chosen from an interval around k, which explains the shift by k in (31).

```
y = initial_guess_of_size(d*(lminus+lplus+1),1);
r = ones(d*(lminus+lplus+1),1);
A = sparse(d*(lminus+lplus+1),d*(lminus+lplus+1));
V = zeros(d*(lminus+lplus+1),1);

while norm(r)>tol
  for i = 0:lminus+lplus-1
    pos =  k-lminus+i;
    A(d*i+1:d*(i+1),d*i+1:d*(i+1)) = -DG(pos,y(d*i+1:d*(i+1)));
    A(d*i+1:d*(i+1),d*(i+1)+1:d*(i+2)) = speye(d,d);
    V(d*i+1:d*(i+1),1) = y(d*(i+1)+1:d*(i+2),1)
                         - G(pos,y(d*i+1:d*(i+1),1));
  end
  A(end-d+1:end,1:d) = speye(d,d);
  A(end-d+1:end,end-d+1:end) = -speye(d,d);
  V(end-d+1:end,1)= y(1:d,1) - y(end-d+1:end,1);
  r = A \ V;
  y = y - r;
end
```

In this program, the vector y contains the finite orbit segment

$$y = \begin{pmatrix} y_{k-\ell_-} & \dots & y_k & \dots & y_{k+\ell_+} \end{pmatrix}^T.$$

It turns out that approximation errors are maximal at the end point of the finite interval J, see [38, Theorem 5 and 8]. The middle part $(y_{k+n})_{n\in\tilde{J}}$ with $\tilde{J} = [n_-, n_+]$, $\ell_- + \gamma_1 \le n_- < n_+ \le \ell_+ - \gamma_2$ provides for sufficiently large $\gamma_{1,2} > 0$ an accurate approximation of $\bar{y}_{\mathbb{Z}}$ for indices around k.

```
bary = y(d*(lminus-nminus)+1:d*(lminus+nplus+1),1);
```

Note that the results as stated in [38] apply for invertible systems only. The techniques utilized in the proofs extend to systems, possessing an exponential dichotomy as defined in Definition 1. Thus, condition (ii) of this definition only requires the system to be regular in the unstable direction.

(2) *Computation of dichotomy projectors at time $k+m$ of the variational equation* (25).

We apply an algorithm that has been introduced in [36, Corollary 1], [37]. Solve for $i = 1, \dots, d$ on the interval $J = [n_-, n_+] \cap \mathbb{Z}$, $m \in J$ the least squares problem

$$\begin{aligned} u^i_{n+1} &= DG_{k+n}(\bar{y}_{k+n})u^i_n + \delta_{n,m-1}e_i, \quad n = n_-, \dots, n_+ - 1, \\ \|(u_n)_{n\in J}\|_2 &= \min . \end{aligned}$$

Here e_i is the ith unit vector and δ denotes the Kronecker symbol.

```
A = zeros(d*(nminus+nplus),d*(nminus+nplus+1));
V = zeros(d*(nminus+nplus),d);

for i = 0:nminus+nplus-1
  pos =  k-nminus+i;
  A(d*i+1:d*(i+1),d*i+1:d*(i+1)) = -DG(pos,bary(d*i+1:d*(i+1)));
  A(d*i+1:d*(i+1),d*(i+1)+1:d*(i+2)) = speye(d,d);
end
V(d*(nminus+m-1)+1:d*(nminus+m),1:d) = speye(d,d);
U = A \ V;
```

If the gap $\min\{|m - n_\pm|\}$ is sufficiently large,

$$\tilde{P}^s_{k+m} := \begin{pmatrix} u^1_m & \dots & u^d_m \end{pmatrix}$$

is an accurate approximation of the dichotomy projector P^s_{k+m}, see [36, Theorem 4.1]. Using this dichotomy projector, we immediately obtain the matrix S_{k+m}.

```
P_k_plus_m = U(d*(nminus+m)+1:d*(nminus+m+1),1:d);
d_s = rank(P,tol); d_u = d-d_s;
S_k_plus_m = [P_k_plus_m*rand(d,d_s),
              (eye(d,d)-P_k_plus_m)*rand(d,d_u)];
Sinv = inv(S_k_plus_m)
```

(3) *The contour algorithm for computing stable fibers.*

Determine in $\tilde{\mathcal{K}}$ the zero-contour, see (30), of

$$H(y) := \tilde{Q}^u S^{-1}_{k+m}\big(\Xi(k+m,k)y - \bar{y}_{k+m}\big) = 0. \tag{32}$$

More precisely, we define a grid Ω on $\tilde{\mathcal{K}}$, evaluate $H(y)$ for $y \in \Omega$ and use these data for an approximation of the zero-contour, employing a contour algorithm. For the latter task, the `contour`-command in MATLAB is a valuable tool that is based on the intermediate value theorem.

```
X = linspace(-2,2,1000);
Y = linspace(-2.5,2.5,1000); % for example
H = zeros(length(Y),length(X));
for i = 1:length(X)
  for j = 1:length(Y)
    y = [X(i);Y(j)];
```

```
      for it = 0:m-1
        y = G(k+it,y);
      end
      z = Sinv*(y-bary(d*(nminus+m)+1:d*(nminus+m+1),1));
      if (abs(z(2,1)) > 10)
        H(j,i) = 10*sign(z(2,1));
      else
        H(j,i) = z(2,1);
      end
    end
  end
  title = ['Stable fiber at time ' num2str(k)];
  figure('name',title)
  contour(X,Y,H,[0 0],'LineWidth',2,'LineColor','g');
```

Note that the graph of H close to its zero contour is rather steep, which makes it hard to apply continuation techniques. Using our approach, seed-points for starting the computation are not needed. In particular, we do not have to care about the number of pre-images in the noninvertible case.

4.3.1 Remarks on the implementation

First, we note that numerical tests suggest that it is advantageous to use a cut-off for large values of H. This is implemented in the previous listing in lines 11 and 12.

Nevertheless, this MATLAB-code can further be optimized, using vectorization techniques. For the purpose of readability, we present non-optimized code snippets in Section 4.3. The optimized code computes one 1D-fiber for the examples, discussed in the next section, in less than one second on a standard computer.

5 Applications

In this section, we present the output of our algorithm for various examples, ranging from autonomous to nonautonomous models and from invertible to non-invertible systems.

5.1 The autonomous Hénon map

Our first example is the well known Hénon map, which plays the role of a normal form for invertible, quadratic two-dimensional mappings, see [32, 50]:

$$G(x) = \begin{pmatrix} 1 + x_2 - a x_1^2 \\ b x_1 \end{pmatrix}. \tag{33}$$

We fix the parameters $a = 1.4$ and $b = 0.3$ and apply the algorithm from Section 4.3 for computing the stable manifold of G w.r.t. the fixed point

$$\xi = \begin{pmatrix} \nu \\ b\nu \end{pmatrix}, \quad \text{where } \nu = \frac{1}{2a}\left(b - 1 + \sqrt{(b-1)^2 + 4a}\right).$$

The diagrams in Figure 2 show for various values of m the sets $\tilde{\mathcal{T}}^m_{G,0}$, i.e. the zero contour of H, which is defined in (32). Corresponding graphs of H are depicted in Figure 3.

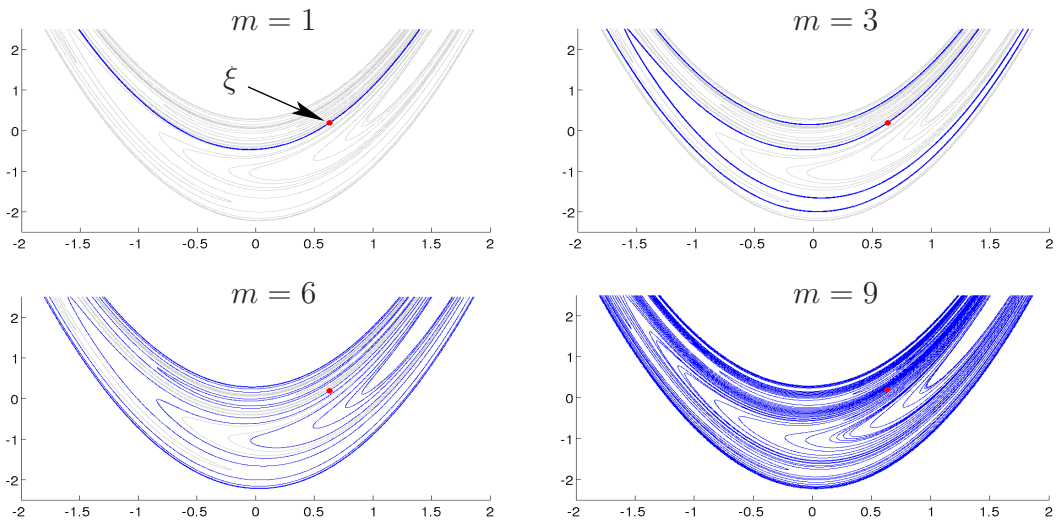

Figure 2: Approximate stable manifolds $\tilde{\mathcal{T}}^m_{G,0}$ (blue) of (33) for various values of m. The gray reference manifold is computed with a shooting algorithm.

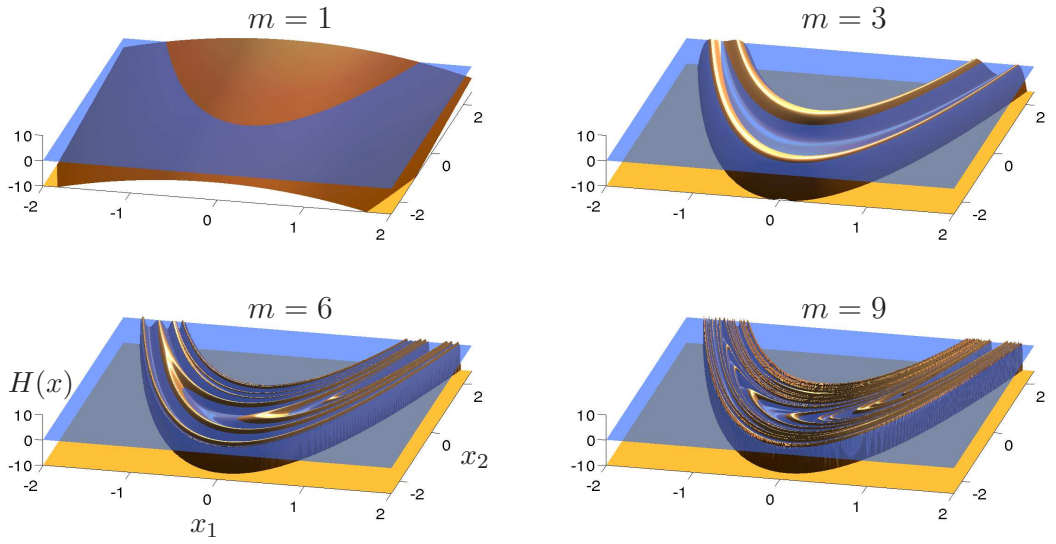

Figure 3: Graphs of H for various values of m. The cut-off plane at -10 is shown in yellow and the zero-plane is shown in blue.

These first tests confirm our theoretical results from Theorem 4, stating that the quality of approximate stable manifolds increases with increasing m. In

Section 5.3 we determine the rate of convergence numerically and compare this results with theoretical expected values. For this task, we construct an example with explicitly known stable fibers.

First, we introduce a nonautonomous extension of the Hénon model.

5.2 The nonautonomous Hénon map

We turn our attention to nonautonomous systems that are invertible. For a first experiment, we revisit the Hénon map (33) and choose the nonautonomous sequence of parameters $a_n = 0.3 + |\sin(n)|$. The bounded trajectory that we compute first, is shown in red in Figure 4. We plot the approximate stable fibers $\tilde{\mathcal{T}}^m_{G,n}$ w.r.t. this bounded trajectory for $m = 6$ and $n = 5, \ldots, 14$. Additionally, we choose 3 points from $\tilde{\mathcal{T}}^6_{G,5}$ and iterate them forward in time. It turns out that these points jump, as expected, from fiber to fiber, converging in this way towards the bounded trajectory.

Note that this hyperbolic system also has an unstable direction. Furthermore, each computed trajectory has – due to numerical errors – a tiny component in this unstable direction. As n increases, this unstable components grows, first unnoticed due to its tininess, but finally it becomes visible.

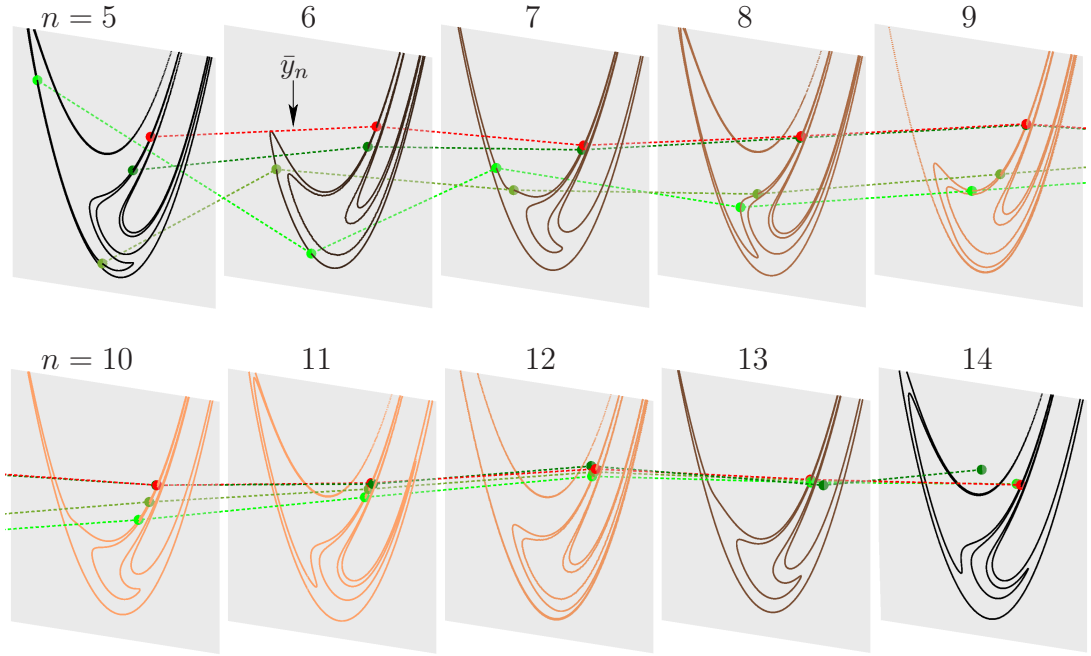

Figure 4: Approximate stable fibers $\tilde{\mathcal{T}}^6_{G,n}$ w.r.t. the bounded trajectory $\bar{y}_{\mathbb{Z}}$ (red) for $n = 5, \ldots, 14$. Three points that are chosen from $\tilde{\mathcal{T}}^6_{G,5}$, are iterated forward in time (shades of green)

5.3 An example with explicitly known stable fibers

We choose in this section an example with explicitly known fiber bundles, see [40, Section 5.1]. The existence of a global reference fiber enables the numerical validation of error estimates of $\tilde{\mathcal{T}}^m_{G,k}$ w.r.t. m.

Consider the family of maps

$$G_n(x) = \begin{pmatrix} \sqrt{a_n}x_1 \\ (a_n+1)x_2 - x_1^2 \end{pmatrix}, \quad a_n \in (0,c),\ c<1, \quad n \in \mathbb{Z}. \tag{34}$$

Stable fiber bundles of the fixed point 0 are given as

$$\mathcal{F}_k = \left\{(x_s, h_k(x_s))^T : x_s \in \mathbb{R}\right\}, \quad h_k(x_s) = x_s^2, \quad k \in \mathbb{Z}$$

and the unstable set is $\left\{(0,x_u)^T : x_u \in \mathbb{R}\right\}$. Note that both, stable and unstable fibers have a global graph representation, cf. [40].

The variational equation w.r.t. the fixed point 0 reads

$$u_{n+1} = \begin{pmatrix} \sqrt{a_n} & 0 \\ 0 & a_n+1 \end{pmatrix} u_n, \quad n \in \mathbb{Z}. \tag{35}$$

Following the proof of Theorem 4, the special structure of (34) allows improved estimates. First, we choose $p=0$, since graph representations are global. Secondly, we find better estimates of h_m in (23):

$$h_m(x_m^s) = (x_m^s)^2 = \left(x_0^s \prod_{i=0}^{m-1} \sqrt{a_i}\right)^2.$$

Denote the stable dichotomy rate of $x^s_{n+1} = \sqrt{a_n}x^s_n$, $n \in \mathbb{Z}$ by α_s then it follows that

$$\operatorname{dist}(\tilde{\mathcal{T}}_k^{m,0}, \mathcal{F}_k) \le K \mathrm{e}^{-(\tilde{\alpha}_u + 2\alpha_s)m}, \quad m \ge 0, \tag{36}$$

with some constant $K>0$. Note that we can choose $\tilde{\alpha}_s < \alpha_s$ arbitrarily close to α_s.

In the autonomous case $a_n = a$ for all $n \in \mathbb{Z}$, (35) has an exponential dichotomy on $\mathbb{Z}$ with rates $\alpha_s = -\log(\sqrt{a})$, $\alpha_u = \log(a+1)$. In Figure 5 we compute $\tilde{\mathcal{T}}^m_{G,0}$ for $a = \frac{1}{2}$, $m \in \{1,5,10\}$ on the set $\Omega = [-1,1]\times[0,1]$. One observes that maximal error occur at the boundary of Ω.

Equation (36) provides an estimate on the expected errors. We verify this estimate by calculating $\operatorname{dist}(\tilde{\mathcal{T}}^m_{G,0}, \mathcal{F}_0)$, via the approximate expression $\sup_{x\in\tilde{\mathcal{T}}^m_{G,0}} \|x_1^2 - x_2\|$, for $m \in [1,12]$ and $a \in \{\frac{1}{10}, \frac{1}{2}, \frac{9}{10}\}$, see Figure 6. Since we compute the contour on a 1000×1000 grid, one cannot expect an accuracy below 10^{-6}, see the left diagram in Figure 6. On the other hand, a high number of iterations may introduce rounding errors that are visible in the right diagram. For computing the exponential slope in Table 1 we only make use of the first 5 data points for

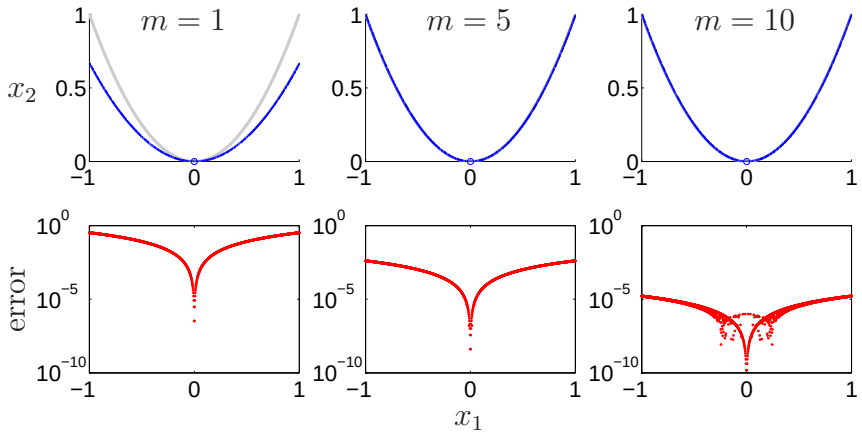

Figure 5: $\tilde{\mathcal{T}}^m_{G,0}$ for $a = \frac{1}{2}$, $m \in \{1, 5, 10\}$ (upper diagrams, reference solution in gray). The lower diagrams show corresponding pointwise errors.

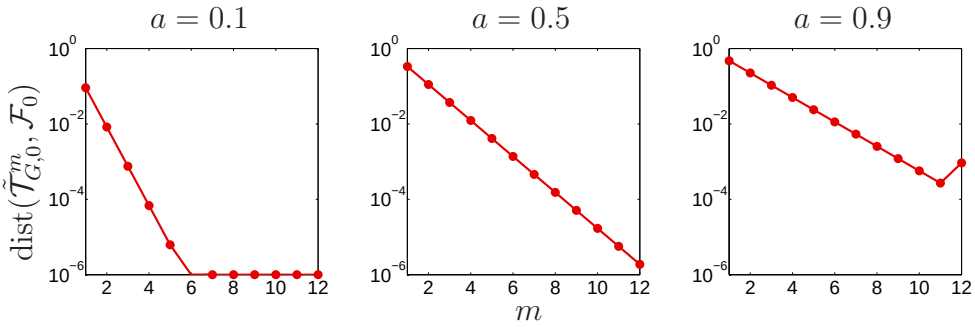

Figure 6: $\mathrm{dist}(\tilde{\mathcal{T}}^m_{G,0}, \mathcal{F}_0)$, $m \in [1, 12]$ for three values of a.

$a = 0.1$ and the first 11 data points for $a = 0.9$. The resulting rates of convergence support our error estimate (36).

We now turn to the nonautonomous case by choosing $a_n \in (0, 1)$ at random uniformly distributed and independent. By the strong law of large numbers, see [43, Theorem 3.23], the following means converge almost surely towards the dichotomy rates $\alpha_{s,u}$:

$$\alpha_s = -\lim_{N\to\infty} \frac{1}{2N+1} \sum_{i=-N}^{N} \log(\sqrt{a_i}) = -\int_0^1 \log(\sqrt{a}) da = \frac{1}{2},$$

$$\alpha_u = \lim_{N\to\infty} \frac{1}{2N+1} \sum_{i=-N}^{N} \log(a_i + 1) = \int_0^1 \log(a+1) da = \log(4) - 1 \approx 0.3863.$$

For a short realization of the random process, one cannot expect to observe these rates in numerical computations. We compute the approximate fiber $\tilde{\mathcal{T}}^m_{G,0}$ for

a	α_s	α_u	$2\alpha_s + \alpha_u$	log. slope dist$(\tilde{\mathcal{T}}^m_{G,0}, \mathcal{F}_0)$
0.1	1.151	0.0953	2.3973	2.3979
0.5	0.3466	0.4055	1.0987	1.0986
0.9	0.0527	0.6419	0.7473	0.7473

Table 1: Estimated and numerically computed errors.

$m \in [1, 10]$ and thus only need 10 random values for this approximation. Finite-time dichotomy rates

$$\tilde{\alpha}_s = -\frac{1}{10}\sum_{i=0}^{9} \log(\sqrt{a_i}), \quad \tilde{\alpha}_u = \frac{1}{10}\sum_{i=0}^{9} \log(a_i + 1)$$

define in this case the order of convergence. For 3 realizations of the random process, Figure 7 illustrates the decay of errors for the contour method. Corresponding rates are listed in Table 2.

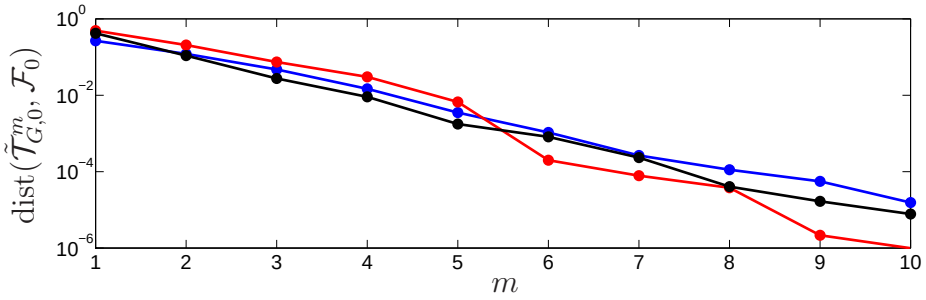

Figure 7: dist$(\tilde{\mathcal{T}}^m_{G,0}, \mathcal{F}_0)$, $m \in [1, 10]$ for three realizations of the random process.

$\tilde{\alpha}_s$	$\tilde{\alpha}_u$	$2\tilde{\alpha}_s + \tilde{\alpha}_u$	log. slope dist$(\tilde{\mathcal{T}}^m_{G,0}, \mathcal{F}_0)$
0.3402	0.4268	1.1072	1.1646
0.4949	0.4148	1.4046	1.4877
0.3869	0.4026	1.1764	1.2817

Table 2: Estimated and numerically computed errors for three realizations of the random process.

5.4 The modified Gumowski-Mira map

In this section, we consider the noninvertible model

$$G_n(x) = \begin{pmatrix} x_2 \\ ax_1 + b_n x_1^2 + x_2^2 \end{pmatrix}, \tag{37}$$

which originates from [27, Equation (2-58)] and is called Gumowski-Mira map in [24, Section 4.3] and [25]. We choose the parameters $a = -0.8$ and $b_n = b \in \{0.1, 0.2\}$ as suggested in the latter references. Then areas with zero and two pre-images exist and this noninvertible map is of type $(Z_0 - Z_2)$, see [51, Section 3.2]. The fixed point ξ, $\xi_1 = \xi_2 = \frac{1-a}{b+1}$ is of saddle type and the stable set consists of one or more closed loops. Figure 8 shows the output of our algorithm for $m = 8$. Note that the computation works automatically and there is no need for the user to first analyze the number of pre-images. Nevertheless, a bifurcation analysis of stable sets explains the occurrence of further loops under parameter variation and can be found in [25].

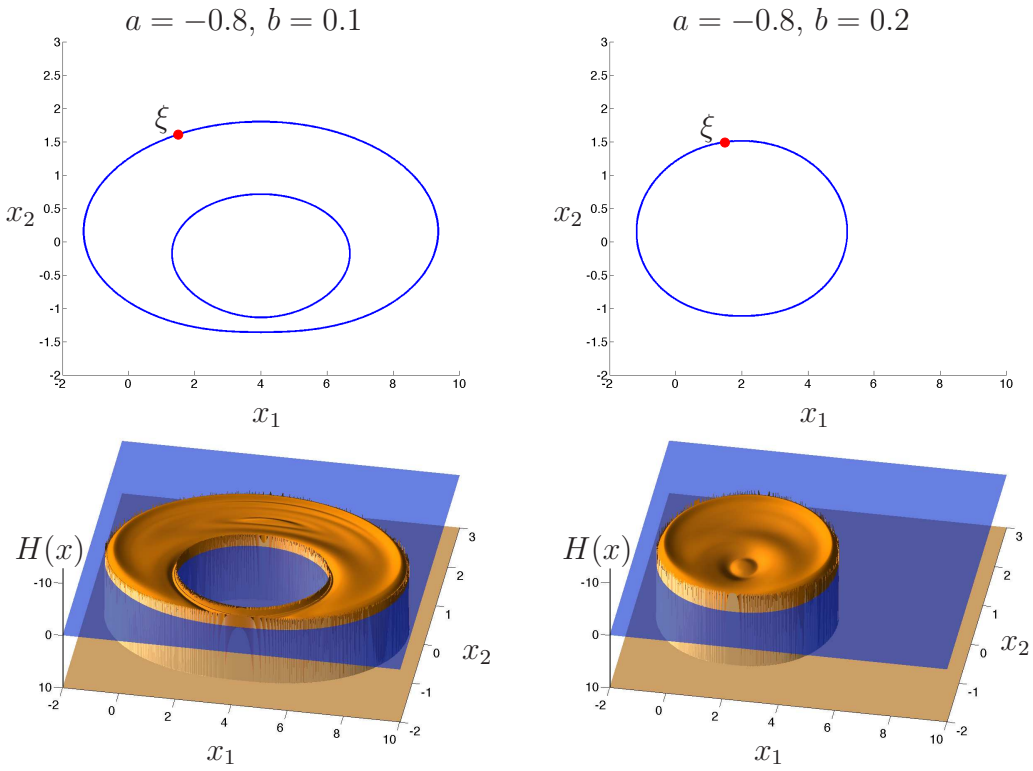

Figure 8: Output of the algorithm from Section 4.3 applied to (37) in case $m = 8$. The lower figures show graphs of H, while their zero-contours are plotted in the upper figures.

For an illustration in a nonautonomous setup, we choose $b_n \in \{0.1, 0.2\}$ at random, see Table 3 and compute stable fibers w.r.t. the bounded trajectory $(\bar{y}_n)_{n\in\mathbb{Z}}$ in Figure 9. Note that $(\bar{y}_n)_{n\in\mathbb{Z}}$ lies in a small common neighborhood of the fixed points for the single parameters. We observe that points, chosen from the fiber at time 0, converge in forward time towards the bounded trajectory until finally, numerical errors cause an increase in the unstable direction. If $b_n = 0.2$, then the stable fiber consists of one closed curve, while we find at time n two

closes curves if $b_n = b_{n+1} = 0.1$. For $b_n = 0.1$ and $b_{n+1} = 0.2$, the stable fiber has a crescentic shape.

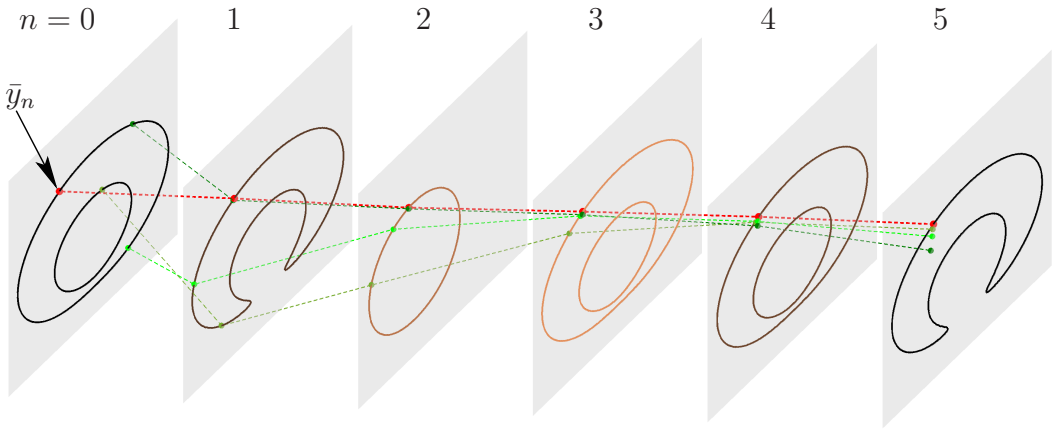

Figure 9: Approximate stable fibers $\tilde{\mathcal{T}}^{10}_{G,n}$ of (37) for $n = 0, \ldots, 5$ of the bounded trajectory $\bar{y}_{\mathbb{Z}}$ (red) together with three points of $\tilde{\mathcal{T}}^{10}_{G,0}$ that are iterated forward in time (shades of green). Corresponding parameters are given in Table 3.

n	0	1	2	3	4	5	6	7	8	9	10
b_n	0.1	0.1	0.2	0.1	0.1	0.1	0.2	0.2	0.2	0.1	0.2

Table 3: Randomly chosen parameters for the computations in Figure 9.

5.5 A model from mathematical finance

The model in this section is noninvertible and the stable set exhibits intersections with itself – a feature that does not occur in previously considered systems. The function

$$G(x) = \begin{pmatrix} x_1 \left(\delta + \frac{1-\delta}{\alpha - x_2}\right) \\ \delta x_2 + (1-\delta) x_1^2 \left(\frac{1}{\alpha - x_2} - 1\right)^2 \end{pmatrix} \tag{38}$$

describes mean (x_1) and variance (x_2) of asset prices in a model with two groups on investors: fundamentalist and chartists. While for the first group, fundamental beliefs determine future asset prices, members of the second group believe only in statistical data for their guess. For a survey on these kind of models, we refer to [14]. The system that we analyze here can be found in [12, Equation (23)], where the presented form (38), exhibits a minimal number of independent parameters. This model is particularly interesting from a dynamical systems perspective, since it possesses homoclinic structures and thus, exhibits chaotic dynamics, see [63], [64, Theorem 5.5].

In the context of this paper, we are interested in the shape of the stable set. For fixed parameters $\alpha = -0.04$, $\delta = 0.8$ we compute $\tilde{\mathcal{T}}^{10}_{G,0}$ w.r.t. the fixed point $\xi = 0$ in Figure 10. Although some local maxima of H have magnitude 10^{-5}, we accurately obtain an approximation of the zero-contour and thus, of $\mathcal{F}_0$.

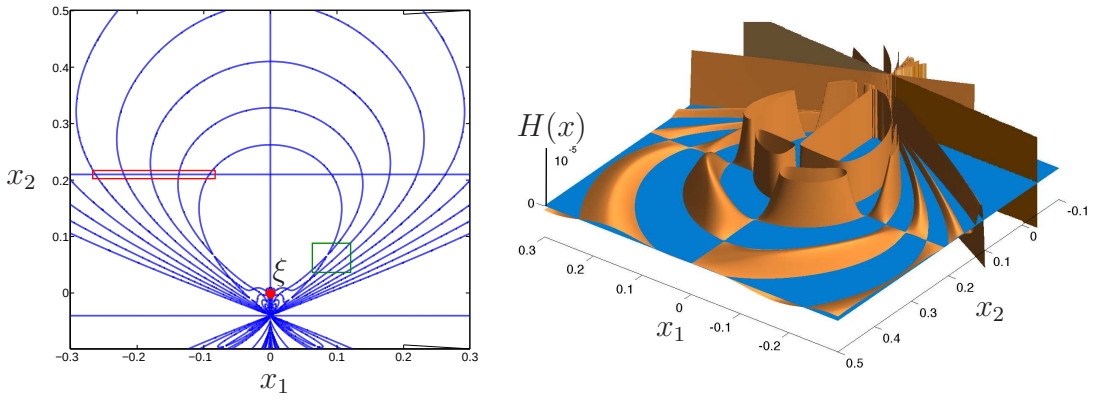

Figure 10: Output of the algorithm from Section 4.3 applied to (38) with $m = 10$. The right diagram shows the graph of H, while its zero-contour is plotted in the left picture. Zooms of the highlighted areas are given in Figure 11.

A closer inspection of Figure 10 (left) reveals some numerical artifacts. These are caused by the `contour`-algorithm in MATLAB that avoids crossing lines, see Figure 11.

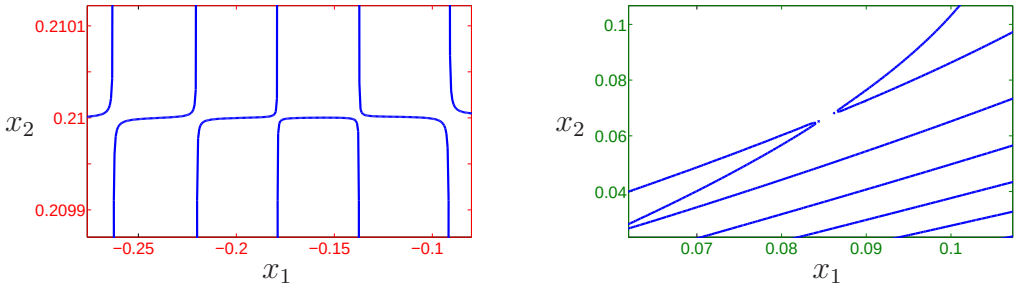

Figure 11: Zoom of the highlighted areas from Figure 10.

For the system (38), we avoid this problem by exploiting the special structure of its stable set:

$$\mathcal{F}_0 = \bigcup_{i=0}^{\infty} \mathcal{W}_i,$$

with

$$\begin{aligned} \mathcal{W}_0 &= \{(0, x_2)^T : x_2 \in \mathbb{R}\}, \\ \mathcal{W}_i &= \{x \in \mathbb{R}^2 : (G^{i-1}(x))_1 \neq 0 \text{ and } (G^i(x))_1 = 0\}, \quad i = 1, 2, \ldots. \end{aligned}$$

For computing these sets explicitly, we observe that

$$(G(x))_1 = 0 \Leftrightarrow \left(x_1 = 0 \quad \text{or} \quad x_2 = \alpha + \frac{1-\delta}{\delta} \right)$$

and consequently $\mathcal{W}_1 = \left\{ \begin{pmatrix} x_1 \\ \alpha + \frac{1-\delta}{\delta} \end{pmatrix} : x_1 \in \mathbb{R} \setminus 0 \right\}$.

Let $x^i = G^i(x^0)$, $i \in \mathbb{N}$, then we iterate this process further and obtain

$$x_1^2 = x_1^1 \left(\delta + \frac{1-\delta}{\alpha - x_2^1} \right) = x_1^0 \left(\delta + \frac{1-\delta}{\alpha - x_2^0} \right) \left(\delta + \frac{1-\delta}{\alpha - x_2^1} \right).$$

The zeros of the last factor (that are not zeros of the first terms) define $\mathcal{W}_2$. The computation of $\mathcal{W}_i$ requires to solve $\delta + \frac{1-\delta}{\alpha - x_2^{i-1}} = 0$ which is again a task for the `contour`-command. These computations are rather involved, since one has to replace x_2^{i-1} iteratively by x_2^0 and this procedure results in highly nonlinear equations.

Figure 12 illustrates the output of this procedure for the same parameter-setup that we choose in Figure 10. One clearly observes that artifacts are avoided successfully. Furthermore, we can increase i further to obtain a more complete picture of the stable set, see Figure 13. It turns out that closed curves occur. Under forward iteration, points on these curves first approach the fixed point ξ, but they make a further excursion before finally converging towards it.

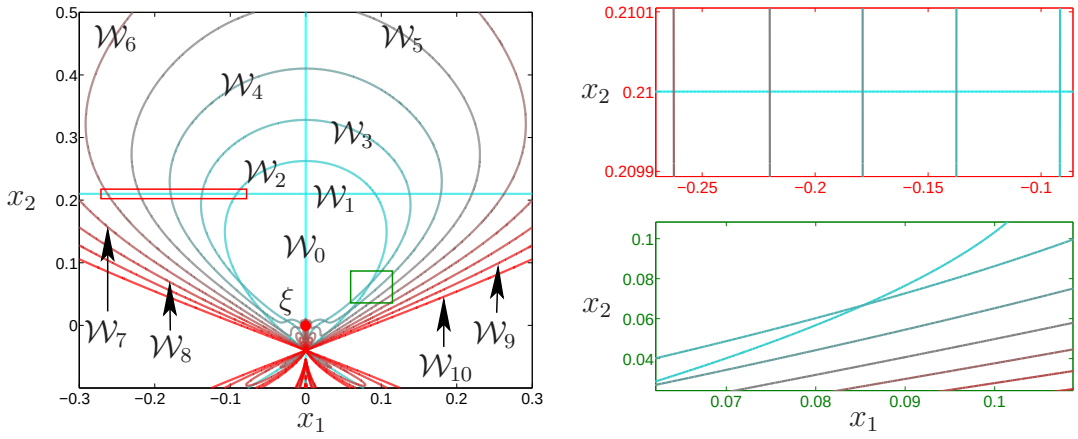

Figure 12: Approximation of $\mathcal{W}_i$ for $i = 0, \ldots, 10$ (left). The right diagrams are zooms of the highlighted areas.

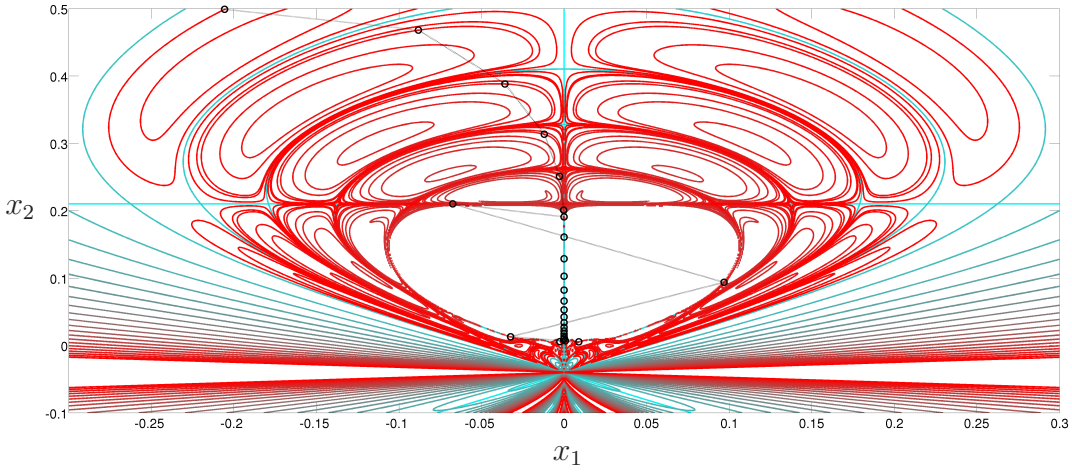

Figure 13: Approximation of $\mathcal{W}_i$ for $i = 0, \ldots, 26$, together with an orbit that starts on $\mathcal{W}_{26}$.

5.6 A two-dimensional stable manifold

We show that the contour algorithm from Section 4.3 can also be used for computing stable fibers in a three-dimensional system. As a prototype, we consider a three-dimensional generalization of the Hénon map, see [10, Example 2]:

$$G(x) = \begin{pmatrix} a + bx_3 - x_1^2 \\ x_1 \\ x_2 \end{pmatrix}, \quad \text{with} \quad a = 1.4,\ b = 0.3. \tag{39}$$

The stable manifold of the fixed point

$$\xi = (z, z, z)^T, \quad z = \frac{b-1}{2} + \sqrt{\frac{(b-1)^2}{4} + a}$$

is two-dimensional. Since the unstable direction is one-dimensional, the graph of H, defined in (32), is 4-dimensional and its zero contour has dimension two. For an approximation of this zero contour, we apply the MATLAB command `isosurface`. The resulting stable manifolds $T^m_{G,0}$ for $m \in \{2, 3, 6\}$ are shown in Figure 14.

5.7 Discussion of degenerate cases

In this section we apply our algorithm to examples that do not satisfy the hyperbolicity Assumption **(A2)**. For this task, we consider modified versions of the system from Section 5.3 that allow explicit studies of approximation errors.

Our models for $i \in \{1, \ldots, 4\}$ are $x_{n+1} = G^i(x_n)$, $n \in \mathbb{Z}$ with

$$G^1(x) = \begin{pmatrix} x_1 \\ 2x_2 - x_1^2 \end{pmatrix}, \quad G^2(x, \alpha) = \begin{pmatrix} \alpha x_1 \\ 2x_2 + (\alpha^2 - 2)x_1^2 \end{pmatrix}, \alpha > 1,$$

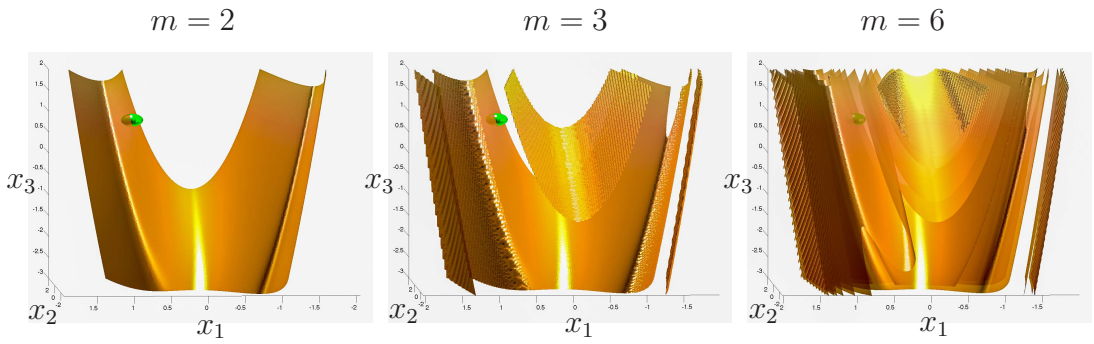

Figure 14: Approximations $T^m_{G,0}$, $m \in \{2, 3, 6\}$, of the two dimensional stable manifold of (39) w.r.t. the fixed point ξ (green ball).

$$G^3(x) = \begin{pmatrix} x_1 + x_1^3 \\ 2x_2 - x_1^2 + 2x_1^4 + x_1^6 \end{pmatrix}, \quad G^4(x) = \begin{pmatrix} x_1 - x_1^3 \\ 2x_2 - x_1^2 - 2x_1^4 + x_1^6 \end{pmatrix}.$$

Figure 15 show sketches of corresponding dynamics. In all examples the x_2 axis and the parabola $\{x \in \mathbb{R}^2 : x_2 = x_1^2\}$ are invariant manifolds. Note that the parabola is a center manifold of $G^{1,3,4}$. We now discuss these examples and the output of the algorithm from Section 4.3 in detail.

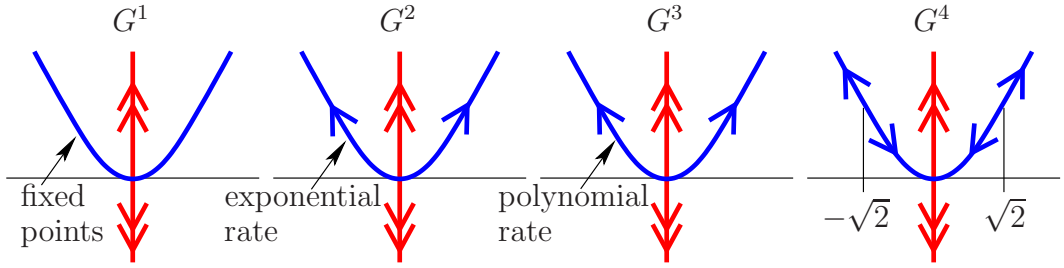

Figure 15: Invariant manifolds of the maps G^i, $i = 1, \ldots, 4$. The arrows illustrate corresponding dynamics on these manifolds.

Starting with G^1, we observe that the parabola, i.e. the center manifold of the fixed point 0 consists of fixed points only. Approximate manifolds $\tilde{\mathcal{T}}^m_{G^1,0}$ are shown in Figure 16 (left), while the right diagram illustrates approximation errors. We compute the exponential slope from the first 9 points in this diagram and get $\log(2)$ with an accuracy of 15 digits.

Note that this example coincides with (34) in case $a_n = 1$ for all n. As a consequence, $\alpha_s = 0$ and we expect from (36) the exponential rate of convergence $\alpha_u = \log(2)$, i.e. exactly the rate that we observe in our numerical experiment.

Generalizing this observation, we may expect convergence of our algorithm if a systems exhibits two unstable directions. The model $G^2(\cdot, \alpha)$ has two unstable rates: $\alpha_{u_1} = \log(2)$ and $\alpha_{u_2} = -\log(\alpha)$. Corresponding invariant manifolds are the x_2-axis and the parabola, respectively. When computing the weakly unstable

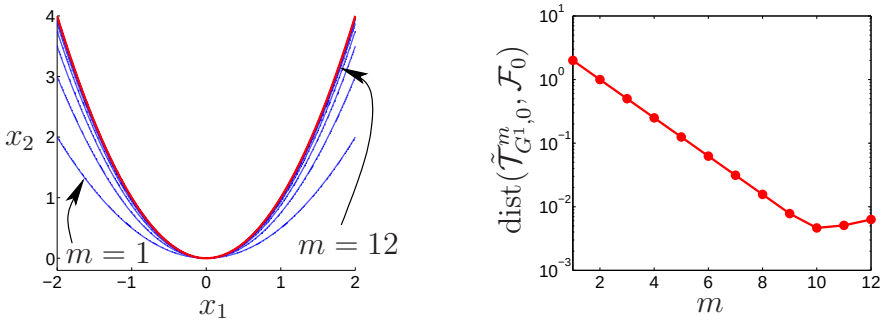

Figure 16: Approximate manifolds $\tilde{\mathcal{T}}^m_{G^1,0}$ (left) and $\mathrm{dist}(\tilde{\mathcal{T}}^m_{G^1,0}, \mathcal{F}_0)$, $m \in [1, 12]$ (right).

manifold, i.e. the parabola, the error estimate (36) indicates convergent behavior as long as

$$-2\alpha_{u_2} + \alpha_{u_1} = -2\log(\alpha) + \log(2) > 0 \quad \Leftrightarrow \quad 0 < \alpha < \sqrt{2}.$$

Figure 17 shows the results of our algorithm for $\alpha_- = 1.41 < \sqrt{2} < 1.42 = \alpha_+$. As predicted, one observes convergence for the parameter α_- with a very slow rate and divergence for α_+.

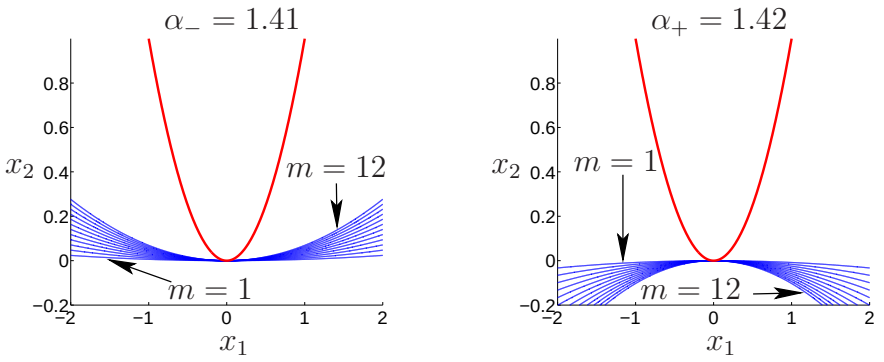

Figure 17: Approximate invariant sets $\tilde{\mathcal{T}}^m_{G^2(\cdot,\alpha_\pm),0}$ for $m \in [1, 12]$.

The third example G^3 also has two unstable directions with different rates of divergence. While the exponential rate on the x_2-axis is constant the dynamics on the parabola is described by the reduced equation $x_1 \mapsto g_c(x_1) = x_1 + x_1^3$. Rates of divergence are polynomially small in a neighborhood of the fixed point, while they dramatically increase for increasing x_1, which is caused by higher order terms. Refining estimate (36), we expect convergence of $\tilde{\mathcal{T}}^m_{G^3,0}$ towards the parabola for values of x_1 satisfying

$$\left|(g_c^m(x_1))^2 \cdot \tfrac{1}{2^m}\right| < 1. \tag{40}$$

The corresponding intervals are shown in Figure 18 (left). The numerically computed sets $\tilde{\mathcal{T}}^m_{G^3,0}$ for $m \in [1, 12]$ are given in the right diagram. We observe that the algorithm possesses the expected convergence behavior.

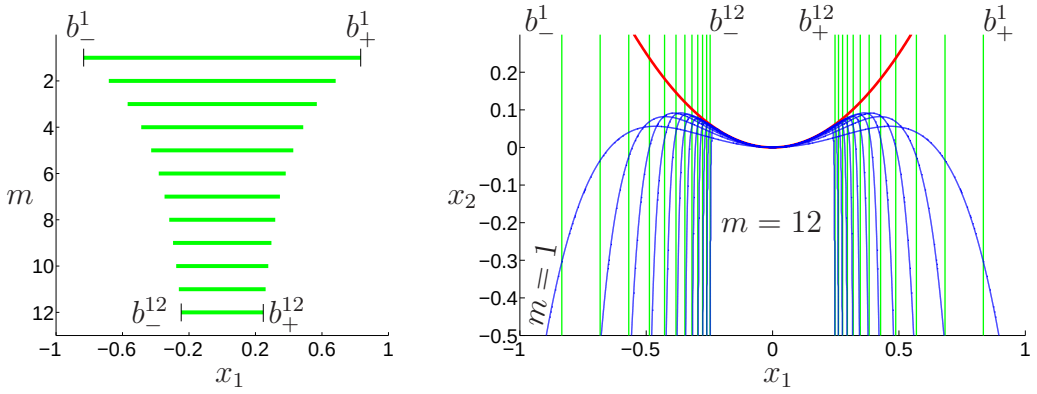

Figure 18: Left diagram: values of x_1 (in green) satisfying (40) for various values of m. Right diagram: approximate invariant sets $\tilde{\mathcal{T}}^m_{G^3,0}$ (in blue) for $m \in [1, 12]$. The green lines indicate the boundaries of the intervals from the left diagram.

Finally, we consider the map G^4. In this example, starting points on the parabola with $|x_1| < \sqrt{2}$ result in orbits that converge towards 0 with a slow, polynomial rate as $n \to \infty$. On the other hand orbits, with starting points on the parabola with $|x_1| > \sqrt{2}$ diverge quickly, as described in the previous example. Thus, we only expect convergence of $\tilde{\mathcal{T}}^m_{G^4,0}$ for $|x_1| < \sqrt{2}$, which is confirmed by our numerical results in Figure 19.

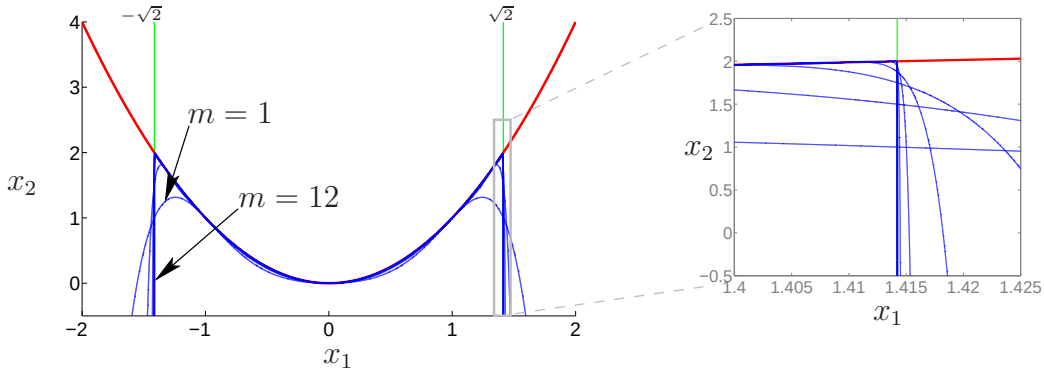

Figure 19: Approximate invariant sets $\tilde{\mathcal{T}}^m_{G^4,0}$ for $m \in [1, 12]$.

6 Conclusion

We propose a contour method for computing stable fibers in discrete time dynamical systems. The resulting algorithm works for nonautonomous and noninvertible models. This is illustrated for examples that show various difficulties:

We start with the invertible Hénon map, exhibiting chaotic dynamics. It turns out that the numerical effort for computing one single fiber for an autonomous and for a nonautonomous setup is identical. Our techniques also apply to a three-dimensional version of this map. We illustrate this by computing its two-dimensional stable manifold.

Stable fibers, having the shape of closed loops occur for the noninvertible Gumowski-Mira map. Numerical computations work automatically without forcing the user to care about the number of pre-images.

A noninvertible model from mathematical finance exhibits stable fibers with self-intersections. Also in this case our approach computes accurate approximations. Furthermore, numerical artifacts that are visible close to points of intersections can be avoided, exploiting the special structure of this system.

Theorem 4 formally justifies our approach. We prove upper semicontinuity of the approximate set w.r.t. the stable fiber and provide precise estimates of approximation errors. For a model with explicitly known fibers, we verify these estimates numerically. Additionally, convergence versus divergence in the presence of center manifolds is discussed.

Finally, we comment on further applications of the contour algorithm. The stable manifold in a model for wild chaos (see [35]) is computed in [9, Figure 8], using the contour algorithm. Applications to ODE-models are discussed in [39], particularly for a two-dimensional damped pendulum equation and for the three-dimensional Lorenz system.

Acknowledgement

The author thanks two anonymous referees for constructive and helpful remarks, which improved the first version of this paper.

References

[1] J.-P. Aubin and H. Frankowska. *Set-valued analysis*. Modern Birkhäuser Classics. Birkhäuser Boston, Inc., Boston, MA, 2009. Reprint of the 1990 edition.

[2] B. Aulbach. The fundamental existence theorem on invariant fiber bundles. *J. Differ. Equations Appl.*, 3(5-6):501–537, 1998.

[3] B. Aulbach and J. Kalkbrenner. Chaotic dynamics from the difference equations point of view. In *Proceedings of the First International Conference on Difference Equations (San Antonio, TX, 1994)*, pages 41–55. Gordon and Breach, Luxembourg, 1995.

[4] B. Aulbach and J. Kalkbrenner. Exponential forward splitting for noninvertible difference equations. *Comput. Math. Appl.*, 42(3-5):743–754, 2001. Advances in difference equations, III.

[5] B. Aulbach, C. Pötzsche, and S. Siegmund. A smoothness theorem for invariant fiber bundles. *J. Dynam. Differential Equations*, 14(3):519–547, 2002.

[6] A. Berger, T. Doan, and S. Siegmund. A remark on finite-time hyperbolicity. *PAMM*, 8(1):10917–10918, 2008.

[7] A. Berger, T. S. Doan, and S. Siegmund. A definition of spectrum for differential equations on finite time. *J. Differential Equations*, 246(3):1098–1118, 2009.

[8] A. Berger, D. T. Son, and S. Siegmund. Nonautonomous finite-time dynamics. *Discrete Contin. Dyn. Syst. Ser. B*, 9(3-4):463–492, 2008.

[9] W.-J. Beyn, T. Hüls, and A. Schenke. Symbolic coding for noninvertible systems: Uniform approximation and numerical computation. 2015. CRC 701, Preprint 15030, Bielefeld University (submitted).

[10] W.-J. Beyn and J.-M. Kleinkauf. Numerical approximation of homoclinic chaos. *Numer. Algorithms*, 14(1-3):25–53, 1997. Dynamical numerical analysis (Atlanta, GA, 1995).

[11] W.-J. Beyn and W. Kleß. Numerical Taylor expansions of invariant manifolds in large dynamical systems. *Numer. Math.*, 80(1):1–38, 1998.

[12] V. Böhm, C. Chiarella, X.-Z. He, and T. Hüls. A homoclinic route to volatility: dynamics of asset prices under autoregressive forecasting. In *Global analysis of dynamic models in economics and finance*, pages 289–316. Springer, Heidelberg, 2013.

[13] X. Cabré, E. Fontich, and R. de la Llave. The parameterization method for invariant manifolds. III. Overview and applications. *J. Differential Equations*, 218(2):444–515, 2005.

[14] C. Chiarella, R. Dieci, and X.-Z. He. Heterogeneity, market mechanisms, and asset price dynamics. In T. Hens and K. R. Schenk-Hopp, editors, *Handbook of Financial Markets: Dynamics and Evolution*, pages 277 – 344. North-Holland, San Diego, 2009.

[15] F. Colonius and W. Kliemann. *The dynamics of control*. Systems & Control: Foundations & Applications. Birkhäuser Boston, Inc., Boston, MA, 2000. With an appendix by Lars Grüne.

[16] W. A. Coppel. *Dichotomies in Stability Theory*. Springer-Verlag, Berlin, 1978. Lecture Notes in Mathematics, Vol. 629.

[17] J. L. Daleckiĭ and M. G. Kreĭn. *Stability of Solutions of Differential Equations in Banach Space*. American Mathematical Society, Providence, R.I., 1974. Translated from the Russian by S. Smith, Translations of Mathematical Monographs, Vol. 43.

[18] R. de la Llave and H. E. Lomelí. Invariant manifolds for analytic difference equations. *SIAM J. Appl. Dyn. Syst.*, 11(4):1614–1651, 2012.

[19] M. Dellnitz, G. Froyland, and O. Junge. The algorithms behind GAIO – Set oriented numerical methods for dynamical systems. In *Ergodic theory, analysis, and efficient simulation of dynamical systems*, pages 145–174, 805–807. Springer, Berlin, 2001.

[20] M. Dellnitz and A. Hohmann. A subdivision algorithm for the computation of unstable manifolds and global attractors. *Numer. Math.*, 75(3):293–317, 1997.

[21] T. S. Doan, K. Palmer, and S. Siegmund. Transient spectral theory, stable and unstable cones and Gershgorin's theorem for finite-time differential equations. *J. Differential Equations*, 250(11):4177–4199, 2011.

[22] L. H. Duc and S. Siegmund. Hyperbolicity and invariant manifolds for planar nonautonomous systems on finite time intervals. *Internat. J. Bifur. Chaos Appl. Sci. Engrg.*, 18(3):641–674, 2008.

[23] T. Eirola and J. von Pfaler. Numerical Taylor expansions for invariant manifolds. *Numer. Math.*, 99(1):25–46, 2004.

[24] J. P. England, B. Krauskopf, and H. M. Osinga. Computing one-dimensional stable manifolds and stable sets of planar maps without the inverse. *SIAM J. Appl. Dyn. Syst.*, 3(2):161–190 (electronic), 2004.

[25] J. P. England, B. Krauskopf, and H. M. Osinga. Bifurcations of stable sets in noninvertible planar maps. *Internat. J. Bifur. Chaos Appl. Sci. Engrg.*, 15(3):891–904, 2005.

[26] N. Fenichel. Persistence and smoothness of invariant manifolds for flows. *Indiana Univ. Math. J.*, 21:193–226, 1971/1972.

[27] I. Gumowski and C. Mira. *Recurrence and discrete dynamic systems*, volume 809 of *Lecture Notes in Mathematics*. Springer, Berlin, 1980.

[28] J. Hadamard. Sur l'itératio et les solutions asymptotiques des équations différentielles. *Bull. Soc. Math. France*, 29:224–228, 1901.

[29] G. Haller. Finding finite-time invariant manifolds in two-dimensional velocity fields. *Chaos*, 10(1):99–108, 2000. Chaotic kinetics and transport (New York, 1998).

[30] G. Haller. Lagrangian structures and the rate of strain in a partition of two-dimensional turbulence. *Phys. Fluids*, 13(11):3365–3385, 2001.

[31] G. Haller. Lagrangian coherent structures. *Annual Review of Fluid Mechanics*, 47:137–162, 2015.

[32] M. Hénon. A two-dimensional mapping with a strange attractor. *Comm. Math. Phys.*, 50(1):69–77, 1976.

[33] D. Henry. *Geometric Theory of Semilinear Parabolic Equations*. Springer-Verlag, Berlin, 1981.

[34] M. W. Hirsch, C. C. Pugh, and M. Shub. *Invariant manifolds*. Springer-Verlag, Berlin, 1977. Lecture Notes in Mathematics, Vol. 583.

[35] S. Hittmeyer, B. Krauskopf, and H. M. Osinga. Interacting global invariant sets in a planar map model of wild chaos. *SIAM J. Appl. Dyn. Syst.*, 12(3):1280–1329, 2013.

[36] T. Hüls. Numerical computation of dichotomy rates and projectors in discrete time. *Discrete Contin. Dyn. Syst. Ser. B*, 12(1):109–131, 2009.

[37] T. Hüls. Computing Sacker-Sell spectra in discrete time dynamical systems. *SIAM J. Numer. Anal.*, 48(6):2043–2064, 2010.

[38] T. Hüls. Homoclinic trajectories of non-autonomous maps. *J. Difference Equ. Appl.*, 17(1):9–31, 2011.

[39] T. Hüls. On the approximation of stable and unstable fiber bundles of (non)autonomous ODEs – a contour algorithm. 2016. To appear in *Internat. J. Bifur. Chaos Appl. Sci. Engrg.*

[40] T. Hüls and Y. Zou. On computing heteroclinic trajectories of non-autonomous maps. *Discrete Contin. Dyn. Syst. Ser. B*, 17(1):79–99, 2012.

[41] M. C. Irwin. *Smooth dynamical systems*, volume 17 of *Advanced Series in Nonlinear Dynamics*. World Scientific Publishing Co. Inc., River Edge, NJ, 2001. Reprint of the 1980 original, With a foreword by R. S. MacKay.

[42] J. Kalkbrenner. *Exponentielle Dichotomie und chaotische Dynamik nichtinvertierbarer Differenzengleichungen*, volume 1 of *Augsburger Mathematisch-Naturwissenschaftliche Schriften [Augsburg Mathematical-Scientific Texts]*. Dr. Bernd Wißner, Augsburg, 1994. With a foreword by Bernd Aulbach.

[43] O. Kallenberg. *Foundations of modern probability*. Probability and its Applications (New York). Springer-Verlag, New York, second edition, 2002.

[44] A. Katok and B. Hasselblatt. *Introduction to the modern theory of dynamical systems*, volume 54 of *Encyclopedia of Mathematics and its Applications*. Cambridge University Press, Cambridge, 1995. With a supplementary chapter by Katok and Leonardo Mendoza.

[45] B. Krauskopf and H. M. Osinga. Growing 1D and quasi-2D unstable manifolds of maps. *J. Comput. Phys.*, 146(1):404–419, 1998.

[46] B. Krauskopf, H. M. Osinga, E. J. Doedel, M. E. Henderson, J. Guckenheimer, A. Vladimirsky, M. Dellnitz, and O. Junge. A survey of methods for computing (un)stable manifolds of vector fields. *Internat. J. Bifur. Chaos Appl. Sci. Engrg.*, 15(3):763–791, 2005.

[47] Y. A. Kuznetsov. *Elements of Applied Bifurcation Theory*, volume 112 of *Applied Mathematical Sciences*. Springer-Verlag, New York, third edition, 2004.

[48] J. A. Langa, J. C. Robinson, and A. Suárez. Stability, instability, and bifurcation phenomena in non-autonomous differential equations. *Nonlinearity*, 15(3):887–903, 2002.

[49] A. M. Mancho, D. Small, S. Wiggins, and K. Ide. Computation of stable and unstable manifolds of hyperbolic trajectories in two-dimensional, aperiodically time-dependent vector fields. *Phys. D*, 182(3-4):188–222, 2003.

[50] C. Mira. *Chaotic dynamics*. World Scientific Publishing Co., Singapore, 1987. From the one-dimensional endomorphism to the two-dimensional diffeomorphism.

[51] C. Mira, L. Gardini, A. Barugola, and J.-C. Cathala. *Chaotic dynamics in two-dimensional noninvertible maps*, volume 20 of *World Scientific Series on Nonlinear Science. Series A: Monographs and Treatises*. World Scientific Publishing Co., Inc., River Edge, NJ, 1996.

[52] K. Nipp and D. Stoffer. *Invariant manifolds in discrete and continuous dynamical systems*, volume 21 of *EMS Tracts in Mathematics*. European Mathematical Society (EMS), Zürich, 2013.

[53] J. Palis, Jr. and W. de Melo. *Geometric theory of dynamical systems*. Springer-Verlag, New York-Berlin, 1982. An introduction, Translated from the Portuguese by A. K. Manning.

[54] K. J. Palmer. Exponential dichotomies, the shadowing lemma and transversal homoclinic points. In *Dynamics reported, Vol. 1*, pages 265–306. Teubner, Stuttgart, 1988.

[55] K. J. Palmer. A finite-time condition for exponential dichotomy. *J. Difference Equ. Appl.*, 17(2):221–234, 2011.

[56] O. Perron. Die Stabilitätsfrage bei Differentialgleichungen. *Math. Z.*, 32(1):703–728, 1930.

[57] C. Pötzsche. *Geometric theory of discrete nonautonomous dynamical systems*, volume 2002 of *Lecture Notes in Mathematics*. Springer-Verlag, Berlin, 2010.

[58] C. Pötzsche and M. Rasmussen. Taylor approximation of invariant fiber bundles for nonautonomous difference equations. *Nonlinear Anal.*, 60(7):1303–1330, 2005.

[59] C. Pötzsche and M. Rasmussen. Taylor approximation of integral manifolds. *J. Dynam. Differential Equations*, 18(2):427–460, 2006.

[60] C. Pötzsche and M. Rasmussen. Computation of nonautonomous invariant and inertial manifolds. *Numer. Math.*, 112(3):449–483, 2009.

[61] C. Pötzsche and M. Rasmussen. Computation of integral manifolds for Carathéodory differential equations. *IMA J. Numer. Anal.*, 30(2):401–430, 2010.

[62] M. Shub. *Global stability of dynamical systems*. Springer-Verlag, New York, 1987. With the collaboration of Albert Fathi and Rémi Langevin, Translated from the French by Joseph Christy.

[63] L. P. Šil'nikov. Existence of a countable set of periodic motions in a neighborhood of a homoclinic curve. *Dokl. Akad. Nauk SSSR*, 172:298–301, 1967. Soviet Math. Dokl. 8 (1967), 102–106.

[64] S. Smale. Differentiable dynamical systems. *Bull. Amer. Math. Soc.*, 73:747–817, 1967.

[65] S. Wiggins. *Normally hyperbolic invariant manifolds in dynamical systems*, volume 105 of *Applied Mathematical Sciences*. Springer-Verlag, New York, 1994. With the assistance of György Haller and Igor Mezić.